A tactile discrimination task to study neuronal dynamics in freely-moving mice

Filippo Heimburg*[,1] , Nadin Mari Saluti*[,1], Josephine Timm*[,1,2], Avi Adlakha [3], Melina Castelanelli [1], Matthias Klumpp [1], Lee Embray [1], Martin Both [1], Andreas Draguhn [1], Thomas Kuner [3] and Alexander Groh [1]

*contributed equally
[1] Institute for Physiology and Pathophysiology, Heidelberg University, 69120, Germany

[2] Current address: Institute for Experimental Epileptology and Cognition Research, University of Bonn, 53105, Germany
[3] Institute for Anatomy and Cell Biology, Heidelberg University, 69120, Germany
groh@uni-heidelberg.de (AG)

Abstract

Sensory discrimination tasks are valuable tools to study neuronal mechanisms of perception and learning. Most of the previously developed discrimination tasks for electrophysiological and imaging studies in rodents require the animals to be head-fixed. However, implementing neurophysiological recordings into more ethologically realistic settings with unrestrained animals has been challenging, especially for somatosensory studies. This study introduces a tactile discrimination task for freely moving mice, integrating electrophysiology and calcium imaging with cellular resolution. In this go/no-go paradigm, mice learn to discriminate between different aperture widths within days in order to forage for food rewards on a linear platform. We demonstrate that the task is whisker-dependent and that mice reliably discriminate aperture differences as small as 6 mm. The setup's versatility enables exploration into diverse behavioral aspects, including tactile discrimination thresholds, valence-dependent behavior, and cognitive flexibility following repeated task rule reversals. Rule learning was highly stereotypical, fast and reproducible across individual mice, with approximately 500 trials to attain expert level performance and approximately 1000 trials to relearn the first rule reversal. We further demonstrate that electrophysiological recordings and calcium imaging can be conducted in the same paradigm such that multiple behavioral read-outs (learning progression, whisker motion, whisker touch, reward licking) can be synchronized with respective electrophysiological and imaging data, providing a new versatile tool to elucidate neural mechanisms of cognition and sensory processing.

Introduction

The rodent whisker system serves as a prevalent model for studying somatosensation in the mammalian brain. A large body of electrophysiological and imaging studies in the whisker system has provided fundamental insights into the mechanisms of sensory perception, learning, and neuronal coding at the single neuron and synaptic levels [1–12]. Since the discovery of the whisker-to-cortex system [13], increasingly advanced experimental approaches have been devised to elucidate the biology and behavioral function of whiskers, while remaining compatible with high-resolution neurophysiological recordings. The most advanced current

state-of-the-art approaches employ recordings in head-fixed mice or rats, while they learn to report or discriminate sensory stimuli [6,14–19]. However, while the head-fixed approach presents the best current compromise between experimental control and biological relevance, head-fixed paradigms impose a limitation in accounting for a core ethological function of the whiskers: active exploration of the rodent's surroundings.

To overcome this limitation, we developed a go/no-go aperture discrimination task for mice inspired by earlier studies on rats [20,21], and combined the task with state-of-the-art single-unit electrophysiological recordings and miniscope imaging. We made modifications to the original design to accommodate rapid learning in mice, naturalistic behavior (foraging on a linear platform), monitoring of licking and whisker behavior, as well as for the learning of multiple rules within an experimentally accessible timeframe. We show that neuronal activity can be monitored over the course of several learning stages in multiple regions of the whisker system using multi-site tetrode recordings and miniscope imaging in the same behavioral paradigm. Collectively, this paradigm forms the basis for studying neuronal mechanisms underlying learning and cognitive flexibility in freely moving mice.

Results

Tactile discrimination setup and learning paradigm

We developed an ethological paradigm in which freely moving mice learn to discriminate different aperture widths with their whiskers in order to collect food rewards. The behavioral apparatus included a linear track equipped with lick ports (LP) for reward delivery (condensed milk) and loudspeakers for punishment (white noise, 120 dB, random duration between 1 to 3 seconds), both situated at opposite ends of the track. To access the LPs, mice had to navigate through motorized apertures of varying widths (Fig. 1A). To ensure adult mice interacted with the aperture using their whiskers during the passage, we estimated the relevant range of aperture widths to be between 45 and 25 mm. Training sessions were done with ambient lights turned off and LEDs (overhead LEDs, backlights, beam brakes) operating in the infrared (IR) spectrum (850 nm), ensuring that mice did not use visual cues to discriminate apertures.

The session started when the mouse crossed the middle IR beam for the first time (Fig. 1A) during the approach to either of the two apertures. A trial started when one of the outer IR beams was crossed (Fig. 1A). Upon palpating the aperture with their whiskers, mice indicated their choice by either licking or not licking at the LP (Suppl. Video 1-3). The general rule logic for scoring the choices and triggering the outcomes was as follows (Fig. 1B, Table 2): licking in response to the go aperture was considered a "hit" and resulted in reward delivery, while not licking was considered a "miss" and resulted in no outcome. Licking in response to the no-go aperture was considered a "false alarm (FA)" and resulted in punishment, while not licking was considered a "correct rejection (CR)" with no outcome. In a later training stage, we introduced a "neutral" aperture which was equidistant to the go and no-go aperture (i.e., 35 mm) and which resulted in no outcome and no scoring.

The training consisted of multiple training stages with specific criteria required to progress to the next stage (Figure 1C, Table 2). Prior to training, mice underwent food restriction for two days with a target body weight of 85–90 % of the initial body weight, which was maintained throughout the later training stages to increase motivation. During this period, mice underwent handling and LP training in their home cage. LP training was conducted with a dummy LP

connected to a syringe via a flexible tube, and condensed milk was dispensed manually upon licking. During the following habituation stage, in which the apertures remained in the go-state, mice learned to alternate between the two LPs and collect rewards. Habituation was completed after four sessions and at least fifty lick trials, after which mice progressed to learn the initial rule, wherein one aperture was linked to reward and a second aperture was linked to punishment. After mice learned the initial rule, they were trained for eight more sessions with the additional neutral aperture. The neutral stage was followed by the reversed rule stage, with reward and punishment contingencies reversed and the neutral aperture removed. In the final stage, the learned behavior was extinguished by randomizing both the apertures and the outcome. The mice's ability to differentiate between aperture widths was assessed using the discriminability index d-prime (d') (Fig. 1D, first column).

Operation of the setup and data acquisition was controlled by Syntalos [22]. Behavioral data was written into an event list which contained the aperture state and data from the three IR beams and the two LPs (Fig. 1A). Data from the event list was used to calculate the performance (Fig. 1D, first column). Recordings from the two high-speed cameras above each LP were triggered when the mouse crossed the outer beam sensors and ended upon the mouse licking or crossing the center IR beam (Suppl. Video 1, 2). These videos were used to extract whisker-aperture contact times and whisker angles using DeepLabCut [23] (Fig. 1D, second column). An overview camera continuously recorded the entire track (Fig. 1A, Suppl. Video 3) and was used for online and offline inspection of the experiment, such as estimation of the location or speed of the mouse on the track. Syntalos additionally operated and archived the multi-channel electrode recordings and miniscope calcium imaging data (Fig. 1D, last two columns).

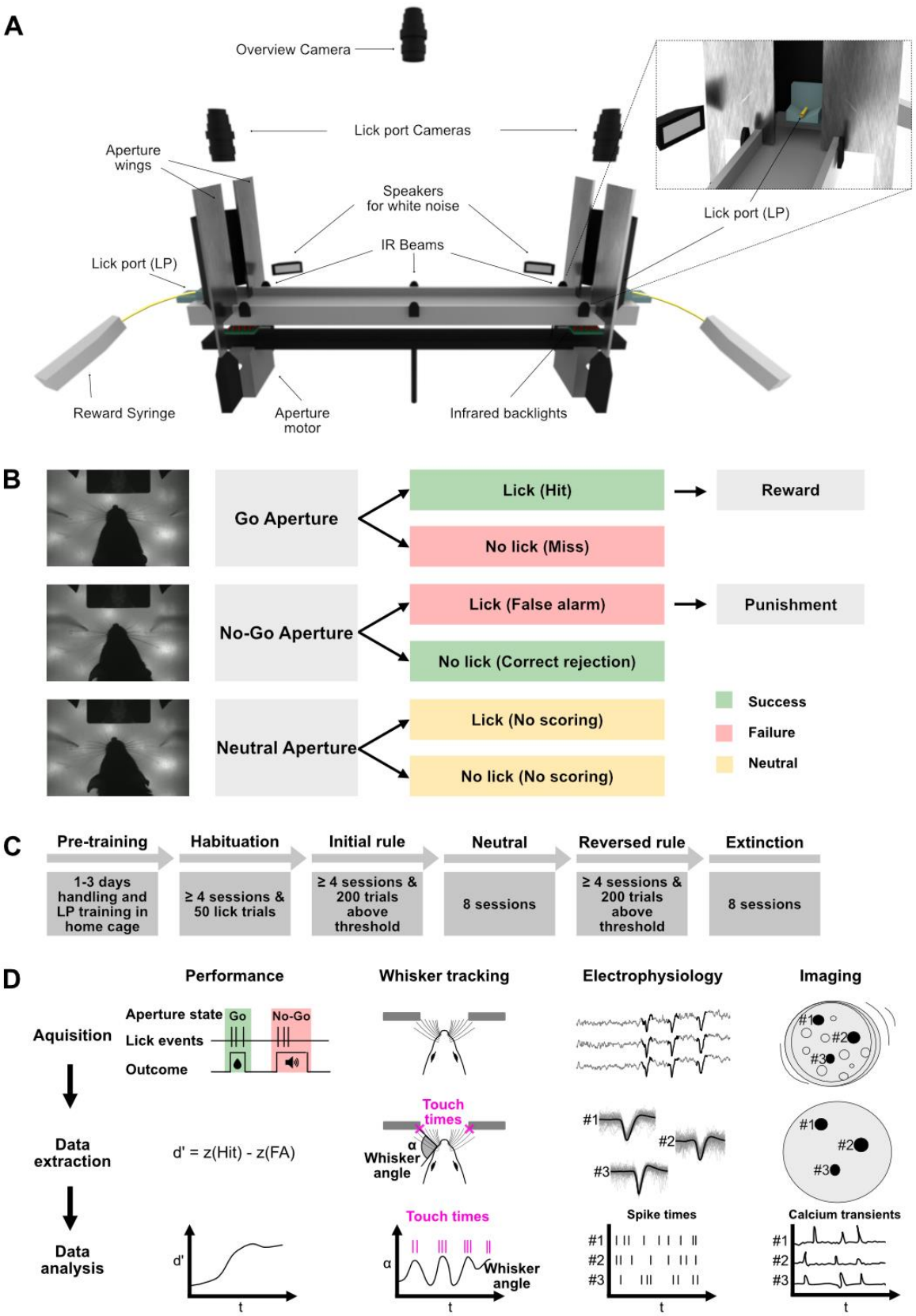

Fig. 1: Tactile discrimination setup and learning paradigm. **A:** Display of the whisker-discrimination setup, created with Blender v2.9 (files can be found here: https://github.com/GrohLab/A-tactile-discrimination-task-to-study-neuronal-dynamics-in-freely-moving-mice [24]). **B:** Rule logic for scoring the choices and triggering the outcomes. **C:** Training scheme with different learning stages and criteria to

move to the next stage. **D:** Overview of data acquisition and analysis pipeline for the analysis of task performance, whisker-aperture touch times, single-unit spike times and calcium transients.

Mice learn to discriminate apertures with their whiskers and learn different task rules

We trained a cohort of 12 mice on the basic training scheme as illustrated in Fig. 1C. Following handling, LP training, and habituation, mice learned the initial rule, wherein the wide aperture (45 mm) was linked to reward and the narrow aperture (25 mm) was linked to punishment (Fig. 1B). On average, mice needed 471 trials (± 128) to surpass the expert-level performance threshold (d' = 1.65) (Fig. 2A). Throughout the learning process, mice more than tripled their activity rate from approximately 20 trials per session in the first four sessions to 60 trials per session in the last four sessions (Fig. 2B). Activity levels remained elevated throughout subsequent training stages (Fig. S1D).

After reaching the expert-level criterion (4 sessions and 200 trials above expert threshold), mice were trained in the reversal stage, in which licking at the wide aperture resulted in punishment and licking at the narrow aperture resulted in reward. In comparison to the initial rule, mice required more than twice the number of trials to learn the reversed rule (471 trials ± 127 vs. 1103 ± 256 trials, Fig. 2C). Similarly, the learning speed, estimated from the slope of a logistic fit of the d' progression, was more than two times slower during reversal learning compared to the initial learning (Fig. 2D). We then investigated in a separate cohort (n = 6) whether mice demonstrate faster relearning of previously learned rules. Indeed, we observed that during repeated rule reversals, mice relearned the rules within fewer trials compared to the first reversal (mean ± standard deviation, 1st reversal: 1078 ± 330 trials, 2nd reversal: 728 ± 144 trials, 3rd reversal: 701 ± 146 trials, Fig. S1C), indicating increased efficiency in relearning repeated rule reversals.

After reaching expert criterion in the reversed rule stage, mice underwent an extinction stage in order to extinguish the previously learned stimulus-outcome associations by randomizing both aperture states and outcomes in each trial (50% chance for “wide”, “narrow”, “reward” and “punishment”). During the extinction stage, mice changed their behavior, such that they always licked, regardless of the aperture state and outcome, resulting in a drop in the discrimination performance to chance level (Fig. 2E).

Finally, we tested the whisker dependency of the task in the following ways. First, in expert animals, we turned off the IR backlights and IR overhead LEDs to test if mice use visual cues. Animals continued to perform at expert level in the no-light condition, demonstrating that visual cues were not used to solve the task (Fig. 2F). In contrast, application of a local anesthetic (4% Lidocaine cream) to the whisker pad or complete removal of all whiskers, both deteriorated the performance of expert animals below performance threshold (Fig. 2G, H).

In summary, this paradigm can be used to train mice to discriminate apertures with their whiskers and to learn different task rules. Mice demonstrated the capacity to update their behavior to new reward-punishment contingencies during multiple reversal stages.

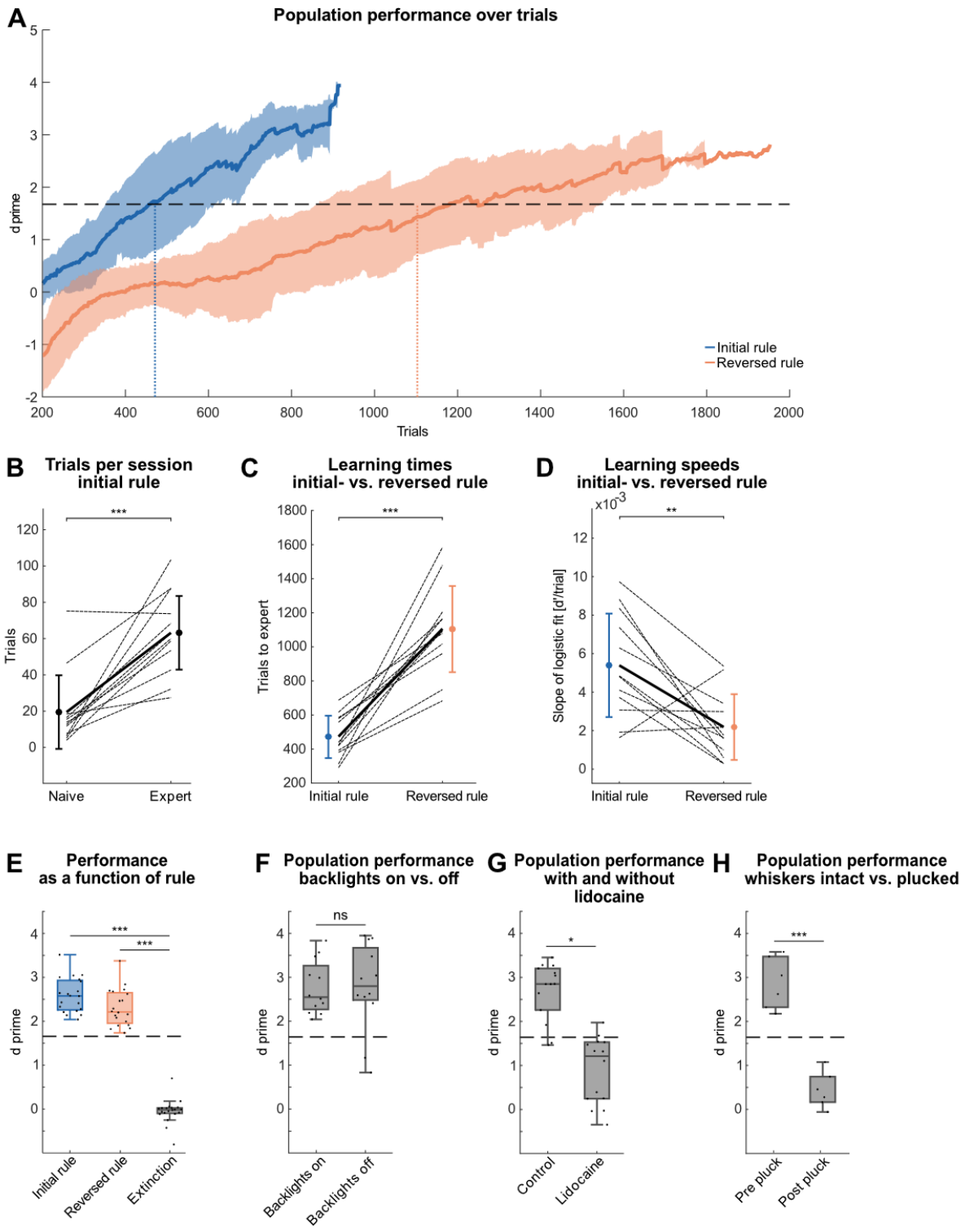
A
Population performance over trials
d prime
Trials
Initial rule
Reversed rule
B
Trials per session initial rule
Trials
Naive
Expert
C
Learning times initial- vs. reversed rule
Trials to expert
Initial rule
Reversed rule
D
Learning speeds initial- vs. reversed rule
Slope of logistic fit [d'/trial]
Initial rule
Reversed rule
E
Performance as a function of rule
d prime
Initial rule
Reversed rule
Extinction
F
Population performance backlights on vs. off
ns
d prime
Backlights on
Backlights off
G
Population performance with and without lidocaine
d prime
Control
Lidocaine
H
Population performance whiskers intact vs. plucked
d prime
Pre pluck
Post pluck

Fig. 2: Mice learn to discriminate apertures with their whiskers and learn different task rules. **A:** Population performance over trials for 20 mm contrast. Solid lines show mean d', calculated with a running window of the preceding 200 trials; shaded areas show standard deviation (initial rule: blue and reversed rule: orange; horizontal line: expert-level performance threshold (d' = 1.65); n = 12 mice). Animals reached expert-level performance after 471 trials in the initial rule stage and after 1103 trials in the reversed rule stage (dotted vertical lines). **B:** Trials per session during the initial rule stage for naive and expert animals (dotted lines: paired values of individual animals; solid line: paired values of population means; data points with error bars: population means and standard deviations; n = 12 mice). **C:** Learning times for initial and reversed rules (same conventions as in B; n = 12 mice). **D:** Learning speeds for initial and reversed rules (same conventions as in B; n = 12 mice). **E:** Population performance for initial rule, reversed rule and extinction. Horizontal line indicates expert-level performance threshold (d' = 1.65). Performance was calculated from the last four sessions in the initial rule and reversed rule stage and the first four sessions in the extinction stage, each dot represents one session, n = 5 mice. **F:** Population performance of expert animals (n = 6 mice) with backlights on and off. Performance was calculated from the last two sessions with backlights on and the first two sessions with backlights off. Same conventions as in E. **G:** Population performance for expert animals (n = 4 mice) with application of lidocaine or neutral ointment (control) to the whisker pad. Performance was calculated from in total 14 sessions across all mice for each condition. Same conventions as in E. **H:** Population performance for expert animals (n = 6 mice) before and after plucking the whiskers. Performance was calculated for the last session before and the first session after the whisker pluck. Same conventions as in E.

ns: $p > 0.05$, *: $p \leq 0.05$, **: $p \leq 0.01$ and ***: $p \leq 0.001$; **B-D, H:** two-tailed paired t-test, **E-G:** repeated measures anova. For exact p values see Supplementary Table 1.

Mice discriminate different aperture contrasts with learning time increasing as contrast decreases

We investigated the minimal aperture contrast that mice can robustly discriminate. We trained a cohort of eight animals on the previous stimulus set which has a contrast of 20 mm (wide = 45 mm; narrow = 25 mm). Subsequently, the contrast was reduced by steps of 4 mm and then by 2 mm. Animals were required to reach the expert-level criterion at each contrast before progressing to the next smaller contrast. We determined the smallest discriminable contrast at 6 mm, below which performance dropped below the expert-level performance threshold. At a contrast of 2 mm, performance dropped to chance level (Fig. 3A).

Next, we trained three additional naive cohorts, each on a different contrast (12, 14, 16 mm), in order to determine the learning times for different contrasts. We found that animals trained on a wider contrast need fewer trials to learn the rules compared to animals trained on a narrower contrast (Fig. 3B, Figure S2). For the 16 mm contrast, mice required an average of 701 ± 110 trials (Fig. S2A, blue line) to reach expert-level performance, whereas those trained on 14 mm and 12 mm contrast required 1180 ± 215 trials (Fig. S2B, blue line) and 1356 ± 142 trials (Fig. S2C, blue line), respectively.

We next tested reversal learning for different contrasts. Again, compared to the initial rule stage, animals required more than twice as many trials to relearn the rule during the reversal stage (factor = 2.22, taking all contrasts into account). The factor between contrasts was not statistically different, suggesting that the doubling of learning time was independent of the contrast. Specifically, during the reversal stage, mice required 1633 ± 356 trials to relearn the task with a 16 mm contrast (Fig. S2A, orange line) and 2260 ± 255 trials with a 14 mm contrast (Fig. S2B, orange line).

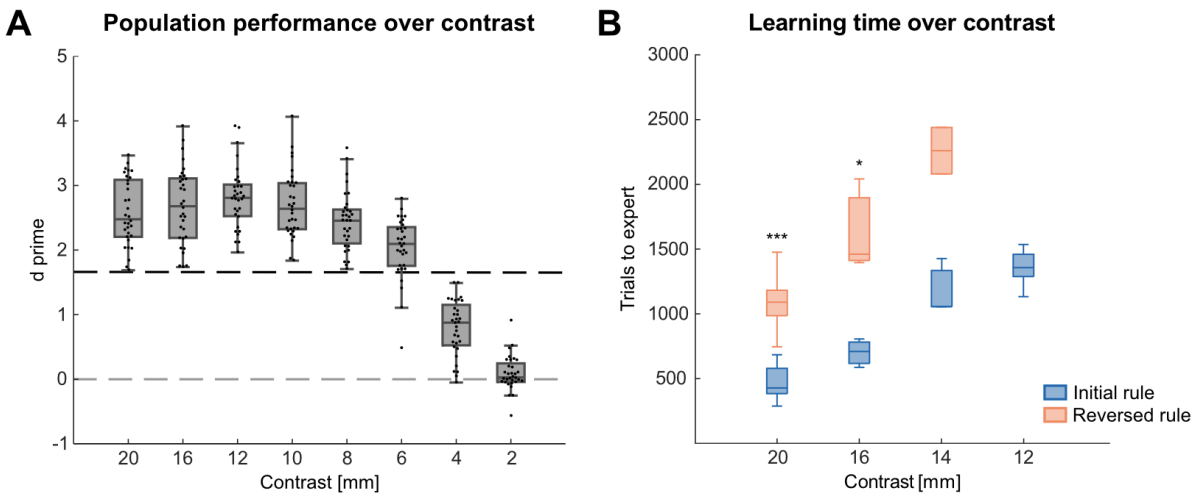

Fig. 3: Mice robustly discriminate aperture contrasts of ≥ 6 mm and learning time increases with smaller contrasts. **A:** Population performance for mice trained on a gradually decreasing contrast. Horizontal lines indicate chance-level and expert-level performance thresholds (d' = 0 vs 1.65, respectively). Performance was calculated from the last four sessions in each contrast condition, each dot represents one session, n = 8 mice. **B:** Number of trials required to reach expert-levels for animals trained on different contrasts in the initial (blue) and reversed rule (orange).

*: $p \leq 0.05$ and ***: $p \leq 0.001$; **B:** paired t-test. For exact p values see Supplementary Table 1.

Mice adapt their behavior during learning

To explore if and how the mice's behavior adapts during learning, we investigated licking and motor behavior in more depth. We first examined lick rates for the different apertures across all subjects over the course of learning. The analysis demonstrated a gradual increase in lick rates for the rewarded aperture and a steep decrease in lick rates for the punished apertures (Fig. 4A). This divergence in lick rates during the initial learning stage indicates the onset of the learning process. The lick rate in response to neutral aperture trials was intermediate between the go and no-go lick rates (Fig. 4A, middle), suggesting that the mice can differentiate between more than two stimuli. During the reversed rule stage, mice initially exhibited inverted lick rates, reflecting their adherence to the previously learned rule. Over time, they gradually adapted to the reversed rule, resulting in a shift toward the correct behavioral response. Notably, in both the initial- and the reversed rule stage, lick rates for the punished aperture dropped after approximately 60% of the learning progression (Fig. 4A), suggesting a stereotypic learning pattern for integrating new rules. Rewarded trials generally showed an earlier lick response compared to punished trials (Fig. 4B), highlighting that learning manifests early on in subtle changes in the licking behavior, before it can be detected with the d' performance measure. As mice gained experience in the task and progressed from naive- to expert-level performance, their lick latencies decreased (Fig. 4C), reflecting enhanced proficiency in task performance. We next explored the mice's movement patterns by projecting a heat map of the positional data along the linear track (Fig. 4D). This analysis revealed that mice spent more time in the sampling and reward areas compared to the openly exposed sections of the maze, reflecting the active exploration in these critical areas of decision-making and a tendency to minimize exposure to open, unprotected spaces. Analysis of the mice's velocity revealed a stereotypical pattern of movement speed, characterized by acceleration toward the middle point and deceleration in front of the apertures before sampling (Fig. 4D).

In summary, the tactile discrimination paradigm can be utilized to study different motor behaviors over the course of tactile discrimination learning. The results demonstrate that learning manifests itself not only in increased tactile discrimination performance but also in an adaptation of motor behaviors.

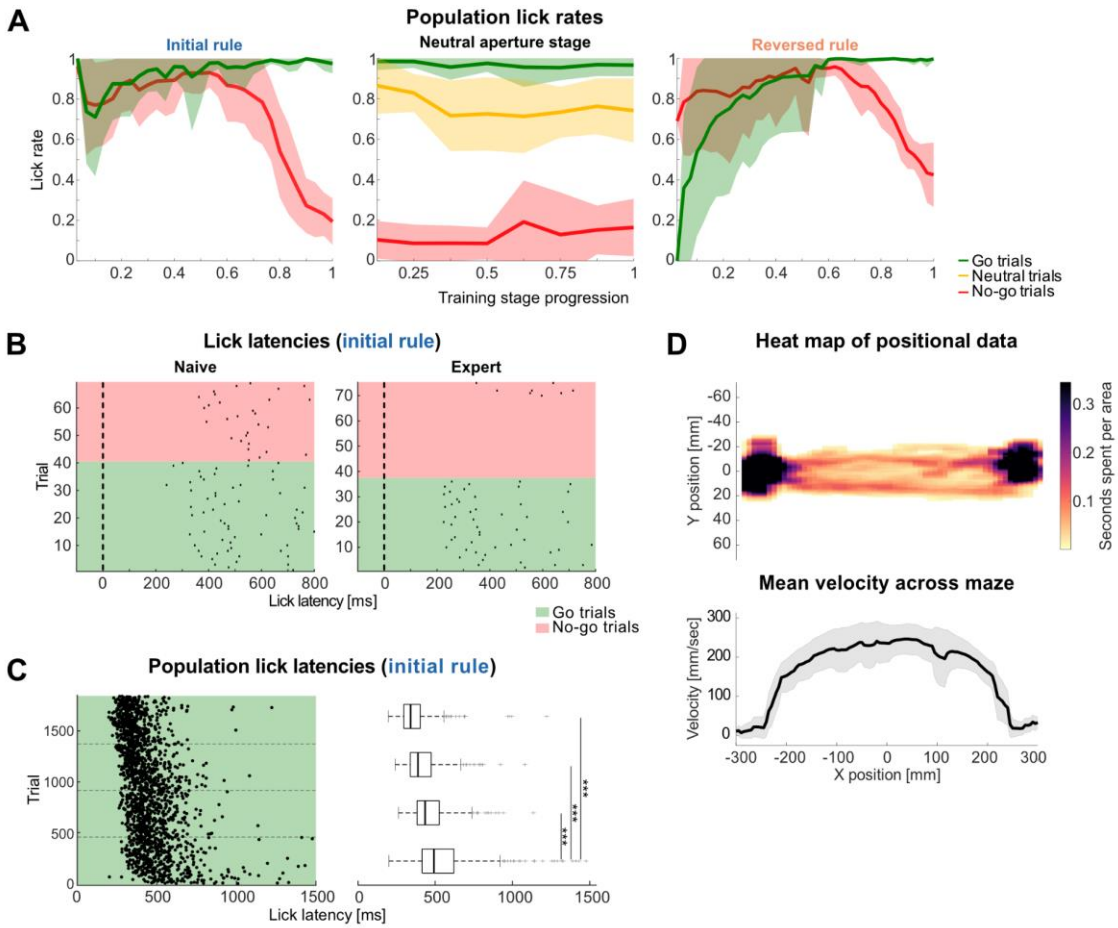

Fig. 4: Adaptation of motor behavior during learning. **A:** Mean lick rates from n = 12 mice across three different stages (initial learning, neutral aperture stage, and reversed rule stage, respectively). **B:** Example lick latencies from one mouse after whisker-aperture interaction (t = 0 ms) for an early- (naive, left) and an expert session (right). **C:** Pooled lick latencies after whisker-aperture interaction (n = 12 mice) across the initial learning stage. Trials were grouped into four equally sized groups for statistical comparison between early (bottom) and late (top) trials. **D:** Heat map of positional data along the linear track of the setup of an exemplary session. The color indicates the time spent in that area (see Methods). The corresponding mean velocity across the track is shown below.

*: $p \leq 0.05$; **C:** Kruskal-Wallis Test. For exact p values see Supplementary Table 1.

Electrophysiological and optical recordings in freely moving mice during tactile discrimination

We explored the versatility of the setup to employ electrophysiological and imaging approaches in the same behavioral paradigm. Therefore, we first implanted tetrode arrays to record simultaneous unit-spiking activity from multiple areas of the somatosensory system in a cohort of 6 mice (Fig. 5A). Tetrode arrays were targeted to the barrel cortex (BC), ventral posteromedial nucleus (VPM), posterior medial complex (POm), and ventral zona incerta (ZIv) (Table 3). Following recovery from surgery, mice were trained in the aperture discrimination

task to expert-level performance. After post-processing the raw electrophysiological data and extracting whisker movements and touch events from the high-speed video recordings, we quantified unit responses (Fig. 5B) as well as population activity in the recorded brain areas (Supplemental Fig. 3A). In expert animals (d' ≥ 1.65), firing rates in about half of the recorded units were modulated by whisker-aperture interactions in all four brain regions. Touch-modulated units comprised 63.2% in the BC (261 out of 413 units, with 53 suppressed and 208 enhanced), 46.1% in the VPM (189 out of 410 units, with 63 suppressed and 126 enhanced), 49.6% in the POm (128 out of 258 units, with 31 suppressed and 97 enhanced), and 60.87% in the ZIv (28 out of 46 units, with 5 suppressed and 23 enhanced).

In addition to electrophysiology, we employed deep-brain calcium imaging (Fig. 5C). We chose the POm as the region of interest because of the recent attention on POm as a thalamic hub for higher cognitive functions [25–29]. To record in vivo calcium signals from the POm, we expressed GCaMP6f in POm via virus injections (Fig. 5D, E). Mice were then trained to reach expert-level performance, and somatic calcium signals were imaged with self-assembled UCLA miniscopes (version 4) attached to an implanted GRIN lens. After post-processing the raw data and extracting the timestamps of whisker touches of the apertures we quantified calcium activity from a total of 541 POm neurons from five expert animals. We found that 20.7% of POm neurons (112/541 neurons) show significant modulation of their activity after whisker-touch (22/112 increased, 90/112 decreased, Fig. 5F-H).

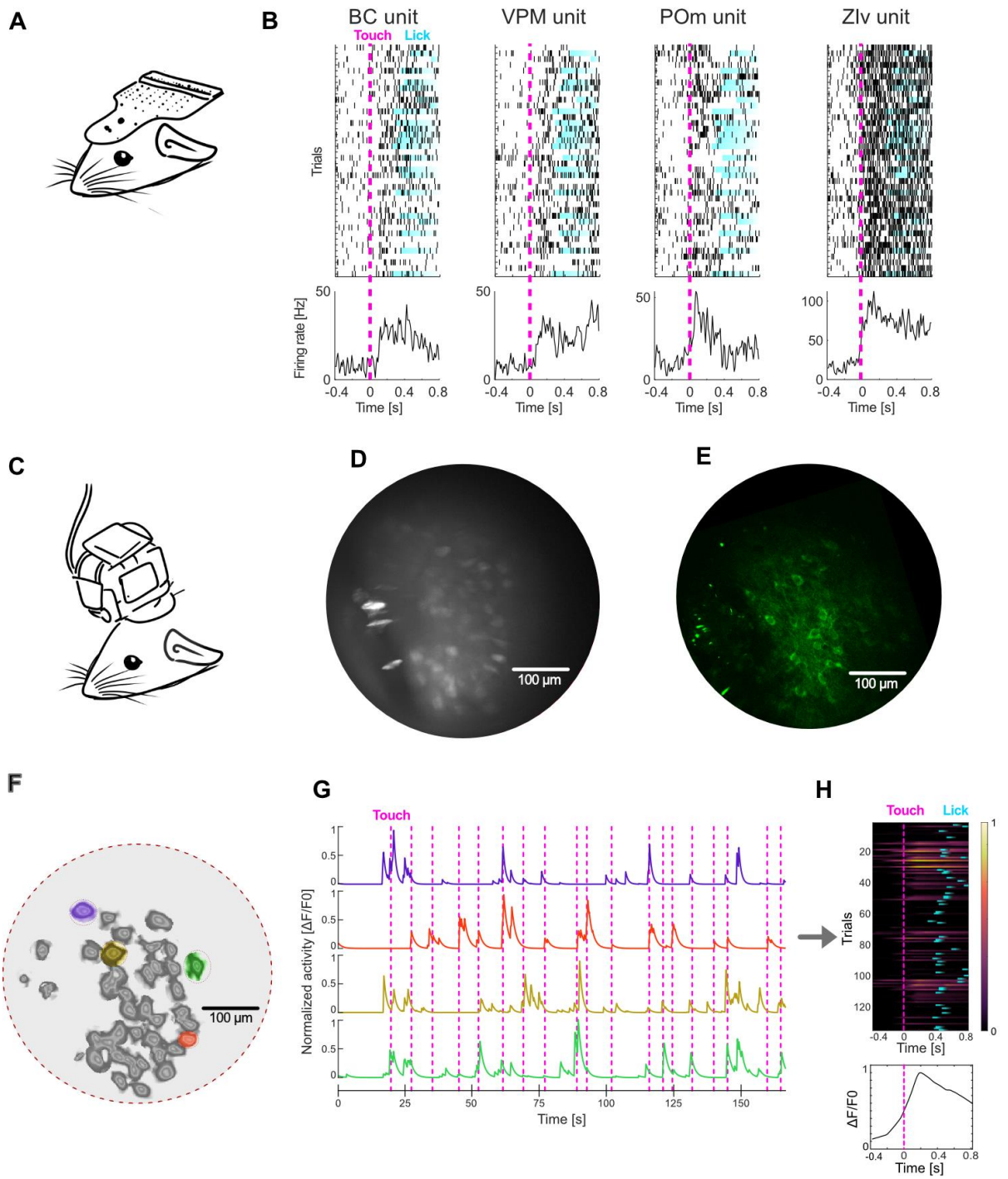

Fig. 5: Neural activity patterns during aperture discrimination task. **A:** Sketch of a head-mounted EIB. **B:** Example raster plots of single unit spiking activity in BC, VPM, POm, and ZIv upon whisker touch of the aperture (magenta line). Lick onset for each trial are marked in blue. Peristimulus time histograms (PSTHs) were min-max normalized and represent the single units' activities during one session. **C:** Sketch of a head-mounted UCLA Miniscope V4. **D:** Example miniscope field of view with POm neurons expressing GCaMP6f. **E:** Field of view of the grin lens imaged with a 2-Photon microscope. **F:** Spatial footprints of the POm neurons detected in one example session. Four example touch-modulated POm neurons are highlighted in color. **G:** Example normalized calcium transients (ΔF/F0) from the four touch-modulated POm neurons in G, magenta lines indicate whisker touches with the aperture. **H:** Normalized calcium transients of the red POm neuron in F and G aligned to whisker touches (magenta) of all trials in one session (top) and averaged across all trials (bottom). Lick onset for each trial are marked in blue.

Aperture states can be decoded from whisker kinematics and from neural activity traces

We next explored whisker-aperture interactions in more detail. To do so, we analyzed the videos of the high-speed cameras above the apertures to capture the dynamics of whisker-aperture contacts during each trial (Fig. 1D). This approach allowed us to calculate the whiskers' kinematic properties, such as speed, curvature, and base angle. Analyzing the whisker angles revealed a rhythmic pattern of whisking at 18.05 ± 3.19 Hz (mean ± std) (Fig. 6A), consistent with previously described whisking frequencies in freely moving mice [30]. When comparing no-go trials between naive (first 4 sessions) and expert sessions (last 4 sessions), we observed that the number of whisking cycles in FA trials remained constant. In contrast, the number of whisking cycles during CR trials were decreased in expert sessions compared to naive sessions (Fig. 6B), indicating that the mice increase their sampling efficiency with learning.

Comparing the mean angular trajectories of the whiskers during narrow and wide aperture trials revealed distinct kinematic signatures, in which – as to be expected from the aperture widths – the whiskers were generally more deflected by the narrow aperture than by the wide aperture (Fig. 6C). We therefore asked whether the aperture state can be predicted from whisker kinematics as the primary metric for a Generalized Additive Model Classifier [31]. Based on these angular trajectories, we could decode the aperture state with high precision, both in sessions where the whisker pad was numbed by lidocaine application and in control sessions where neutral ointment was applied to the whisker pad. Specifically, the decoding accuracies for both lidocaine and control sessions were significantly greater than those obtained with randomly shuffled aperture labels (Fig. 6D). However, the decoding accuracies between lidocaine and control sessions did not differ significantly (Fig. 6D), even though lidocaine interfered with stimulus transmission, thereby impeding proper behavioral responses (Fig. 2G). This suggests that the lack in discrimination cannot be attributed to impaired whisker kinematics.

Using the same decoding approach, we tested, whether the aperture states can also be predicted from spike trains recorded during both control sessions and sessions where lidocaine was applied to the whisker pad. Using the neuronal traces of each brain area as input for the decoding of the apertures, the results revealed accurate prediction of the aperture states in the control sessions (Fig. 6E). However, we observed a significant decrease in decoding accuracy when comparing lidocaine to neutral ointment sessions (Fig. 6E). This suggests that the encoding of aperture widths information in the spike trains was impaired after blocking sensory transmission with lidocaine on the whisker pad.

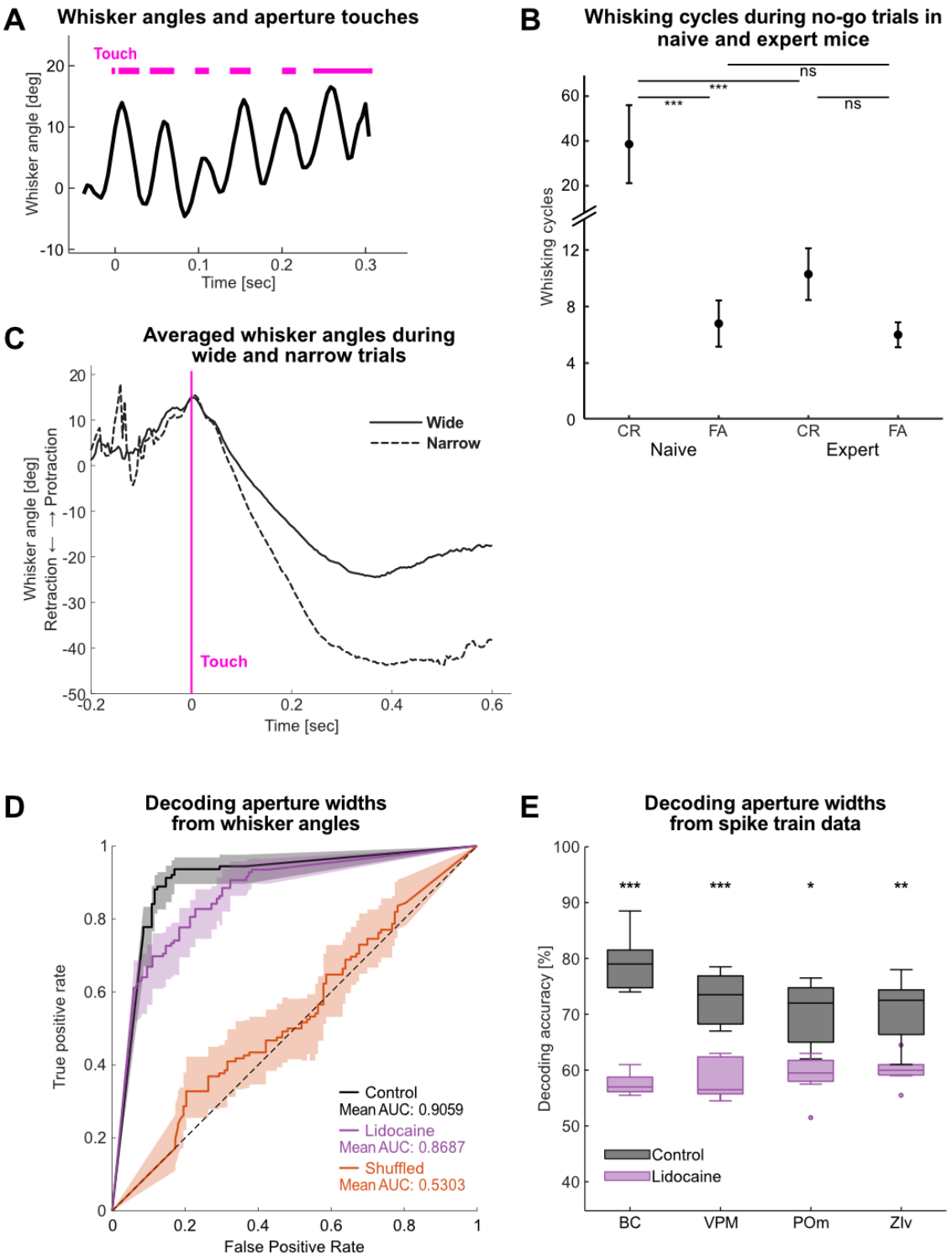
A
Whisker angles and aperture touches
Touch
Whisker angle [deg]
Time [sec]
B
Whisking cycles during no-go trials in naive and expert mice
ns
***
***
ns
Whisking cycles
CR
FA
CR
FA
Naive
Expert
C
Averaged whisker angles during wide and narrow trials
Wide
Narrow
Whisker angle [deg]
Retraction ← → Protraction
Touch
Time [sec]
D
Decoding aperture widths from whisker angles
True positive rate
False Positive Rate
Control
Mean AUC: 0.9059
Lidocaine
Mean AUC: 0.8687
Shuffled
Mean AUC: 0.5303
E
Decoding aperture widths from spike train data
Decoding accuracy [%]
***
***
*
**
Control
Lidocaine
BC
VPM
POm
Zlv

Fig. 6: Decoding of aperture states from whisker kinematics and from neural activity traces. **A**: Example whisker angle and aperture touches (magenta) during a hit trial (averaged angle values α from four DeepLabCut-tracked whiskers). **B**: Number of whisking cycles during no-go trials in naive (initial 4 sessions) and expert sessions (final 4 sessions), n = 6 mice. **C**: Average whisker angles upon encountering (0 ms) the wide (solid) or narrow (dashed) aperture, n = 6 mice. **D**: Receiver operating characteristic (ROC) curves from a generalized additive model (GAM) classifier based on whisker angles after whisker-touch onset. Comparison of control (gray), lidocaine sessions (purple), and randomly shuffled labels (orange). Accuracies for control and lidocaine sessions were not significantly different from each other, but both differed significantly from the shuffled accuracies (n = 6 mice). **E**: Comparison of the classifier decoding accuracy based on neural traces between lidocaine sessions (purple boxes) and control sessions (gray boxes). Number of units (from n = 6 mice) in lidocaine sessions: 128 (BC), 100 (VPM), 52 (POm), 17 (ZIv); and control sessions: 150 (BC), 101 (VPM), 64 (POm), 17 (ZIv).

ns: $p > 0.05$, *: $p \leq 0.05$, **: $p \leq 0.01$ and ***: $p \leq 0.001$; D: two-tailed paired t-test, E: two-tailed Wilcoxon rank sum test. For exact p values see Supplementary Table 1.

Discussion

This study introduces a go/no-go whisker-dependent discrimination paradigm for freely moving mice. Compared to head-fixed paradigms, this novel paradigm enables investigations into mouse behavior and learning in a more natural and unrestrained environment, while being compatible with high-resolution electrophysiology, imaging and motor behavior measurements. The discrimination task relies solely on somatosensory whisker information for aperture discrimination, demonstrated by deteriorated performance when whiskers were anesthetized or removed. Furthermore, compared to texture discrimination tasks [6,17,32–35], in which surface differences are created by switching between different sandpapers, the use of the same apertures with variable widths ensures the elimination of potential confounders from olfactory cues.

Learning speeds and discrimination performance were stereotypical between mice, with fast learning within a total training time of approximately four hours, spread over eight days (two 15-minute sessions per day). This fast learning not only allows for high-throughput behavioral analysis but also provides several other advantages. First, the paradigm allows the incorporation of multiple consecutive learning stages in which mice learn different rules. In the basic training scheme, we trained mice on four stages (initial, neutral, reversed rule, devaluation) within a total of 29 ± 4 days. Second, the paradigm can be used in repeated rule switch mode, by switching back and forth between two inverted rule sets (Fig. S1B, C). This can be advantageous for learning studies that require a steady-state learning environment without confounding learning factors which happen only in the initial learning when mice are exposed to the learning paradigm for the first time. Indeed, we found several behavioral adaptations which happen in the initial learning and then stabilize, for example overall activity (trial counts per session), lick latencies, and overall learning speed, which progressively approached an efficient optimum following multiple rule switches. Most importantly, the fast learning allows for chronic neurophysiology within a short experimental time frame. This is advantageous to monitor neuronal activity over the entire learning period and even during multiple learning rules, which is often difficult to achieve because of the deteriorating signal quality and unit yield in chronic electrophysiological and optical recordings [36–38].

Animals were able to flexibly adapt to changing rules, demonstrating the capacity to update behavior when predicted outcomes of the sensory cues changed. Our results further indicate a faster relearning of previously learned rules (Fig. S1C), a phenomenon known as "savings" from human studies [39,40]. The ability of mice to relearn repeated rules reversals more efficiently suggests the involvement of higher cognitive processes. Further neurophysiological studies in other brain areas, such as prefrontal cortex [6] or motor cortex [41], could help to elucidate the processes of learning and memory consolidation.

Animals could discriminate between different aperture states and demonstrated robust discrimination of aperture contrasts as small as 6 mm, comparable with previous results from rats in a forced-choice setting (smallest discriminable contrast of 3 mm in Krupa et al. 2001 [20]). However, mice can likely discriminate smaller contrasts given the right motivation, as they have been shown to discriminate submillimeter differences in sandpaper textures [33]. In contrast to texture discrimination tasks, where the whiskers interact with fine surface features via stick-slip micromotions [35,42–44] our distance discrimination task likely depends more on whisker-angle changes.

At the beginning of the learning phase of the initial rule and during extinction, mice generally engaged in constitutive licking in each trial, independent of the aperture state. This constitutive licking behavior yields rewards and punishments at a 50% rate and indicates that the motivational value of the reward outweighs the negative impact of the punishment when the outcomes of the aperture states are not predictable.

Electrophysiological and optical recordings revealed touch-modulated single unit responses in multiple brain regions, including the BC, VPM, POm, and ZIv. Using the spike-trains from these recordings allowed for accurate decoding of the aperture width while Lidocaine numbing of the whisker pad significantly impaired decoding. Together this demonstrates that task-relevant information for tactile discrimination is encoded in the thalamocortical system. While we recorded neurophysiological signals throughout the entire training scheme, including several rule sets, here we focus only on expert animals to demonstrate that imaging and electrophysiology can be implemented within the same freely-moving discrimination paradigm. Future studies will explore the neural dynamics during learning for example by studying context-dependent neuronal representations of sensory cues in naive and expert animals or during rule switch mode.

Material & Methods

Product	Supplier
Linear track (82 x 10 cm, wood)	Custom built, Lee Embray, Heidelberg
Controlling unit of the behavioral apparatus (Arduino Uno R3 with firmata firmware)	Arduino, assembled by Lee Embray, Heidelberg
Apertures	
Metal wings (height: 205 mm, width: 97 mm, aluminum)	Lee Embray, Heidelberg
Controlling unit with stepper motors (https://github.com/GrohLab/A-tactile-discrimination-task-to-study-neuronal-dynamics-in-freely-moving-mice/blob/main/MaterialList/ApertureGate/info.md) [24]	Lee Embray, Heidelberg
Lick ports adapted from Cornelius Schwarz, Tübingen [45]	
Vasofix® Safety Braunüle® FEP G16	B. Braun SE, Melsungen, Germany
Piezo sensor (#285-784)	RS components GmbH, Mörfelden-Walldorf, Germany
Analog-to-digital converter (ADC)	Cornelius Schwarz, Tübingen [45]
Sensors and IR illumination	
Light beams (https://github.com/GrohLab/A-tactile-discrimination-task-to-study-neuronal-dynamics-in-freely-moving-mice/blob/main/MaterialList/LightBeams/info.md) [24]	Lee Embray, Heidelberg
LED strips for overhead illumination (Synergy 21 LED Flex Strip infrarot IR 12 12V IP65 Security Line 850nm, #140455)	ALLNET GmbH, Germering, Germany
Backlight LEDs (HT-110IRPJ IR-Emitter 850 nm 140° 1204 SMD)	Harvatek Corporation, Hsinchu, Taiwan
Diffuser plate (3D printed with clear FLGPCL04 and sanded with P600)	Formlabs GmbH, Berlin, Germany
Diffuser film, 60% light diffusion (#DSF-10)	Folien Fischer UG, Hamburg, Germany
Intervention drugs	
Isoflurane (Isofluran Baxter)	Baxter Deutschland GmbH, Germany
Buprenorphine (Bupresol vet. Multidose 0,3 mg/ml, 10 ml)	CP-Pharma Handelsgesellschaft mbH, Burgdorf, Germany
Ketamine (100 mg/ml, 10 ml)	CP-Pharma Handelsgesellschaft mbH, Burgdorf, Germany
Xylazine (Xylavet® 20 mg/ml)	CP-Pharma Handelsgesellschaft mbH, Burgdorf, Germany
Lidocaine (Xylocaine® 1%)	Aspen Pharma Trading Limited, Ireland

ssAAV-1/2-hSyn1-chI-GCaMP6f-WPRE-SV40p(A)	Viral Vector Facility (VVF), Zürich, Switzerland
Cameras	
2x High speed cameras (DMK 37BUX287)	The Imaging Source Europe GmbH, Bremen, Germany
Overview camera (DMK 37BUX290)	The Imaging Source Europe GmbH, Bremen, Germany
Reward / punishment	
Food dispensers (https://github.com/GrohLab/A-tactile-discrimination-task-to-study-neuronal-dynamics-in-freely-moving-mice/blob/main/MaterialList/FoodDispensers/info.md) [24]	Lee Embray, Heidelberg
2 ml syringes (BD Discardit II)	Becton Dickinson GmbH, Heidelberg, Germany
Tubes with Luer connector (#4256000)	B. Braun SE, Melsungen, Germany
Hifi integrated amplifier (A-S301)	Yamaha Music Europe GmbH, Rellingen, Germany
2x Speakers (Neo X 3.0 ribbon tweeter)	Fountek Electronics Co., Ltd, Zhejiang, China
EIB	
RHD USB Interface Board (#C3100)	Intan Technologies, CA, USA
Samtec Male Connector EIB (ST4-40-1.00-L-D-P-TR)	Samtec Europe GmbH, Germering, Germany
Samtec Female Connector Headstage (SS4-40-3.00-L-D-K-TR)	Samtec Europe GmbH, Germering, Germany
PCB (EIB and headstage)	Custom built (BRD file: https://github.com/GrohLab/A-tactile-discrimination-task-to-study-neuronal-dynamics-in-freely-moving-mice/blob/main/MaterialList/EIB64-ST4-Multi.brd) [24], printed by Multi-Circuit-Boards Ltd, Munich, Germany
Tungsten 99.95% CS Wire for Tetrodes (#100211)	California Fine Wire Company, CA, USA
Gold chloride solution for gold plating (200 mg/dL gold chloride in deionized water, HT1004-100ML)	Sigma-Aldrich, Inc., MO, USA
Intan Interface 64 Channel Amplifier Chip (RHD2164)	Intan Technologies, CA, USA
UV-curable adhesive (3M™ Filtek™ Supreme XTE)	3M Deutschland GmbH, Neuss, Germany
Function generator (A365 Stimulus Isolator)	World Precision Instruments, Inc., FL, USA
Electric Rotary Joint (AHRJ-OE_2x2_AD_200-0.22_24_USB-C)	Doric Lenses Inc., Quebec City, Canada
Miniscope V4	
Miniscope V4 main body (Excitation, objective, and emission module)	Custom print from Heidelberg precision mechanics workshop/ Open Ephys

V4 Base Plate	Custom print from Heidelberg precision mechanics workshop/ Open-Ephys
Rigid-Flex PCB	Open-Ephys
Optical Filters - Excitation filter 4mm x 4mm, ET47/40x - Emission filter 4mm x 4mm, ET525/50m - Dichroic mirror 6mm x 4mm, T495lpxr	Chroma/ Open-Ephys
Lenses - 2 x 3mm diameter, 6mm FL achromat used in the objective module (#45-089) - 4mm diameter, 10mm FL achromat used in the emission module (#63-691) - Half-ball Lens, 3.0mm Diameter, N-BK7 (#47-269)	Edmund Optics/ Open-Ephys
Coax cable, 36AWG 26/50SPC	Cooner Wire
Hirose U.FL Connector, U.FL-PR-SMT2.5-1(10)	Mouser
GRIN Lenses, ProView™ Lens Probe, 0.5mm diameter, ~4.0mm length	Inscopix

Table 1: Parts list

Animals

All experimental procedures were approved by the local governing body (Regierungspräsidium Karlsruhe, Germany, approval numbers: 35-9185.81/G-216/19 and 35-9185.82/A-8/20) and performed according to their ethical guidelines. The experiments were done with adult male mice from the inbred strain C57BL/6NRj (Janvier Labs, Le Genest-Saint-Isle, France). Mice were 8-10 weeks old at the start of training, with a mean body weight of 25.94 ± 2.33 g (mean ± standard deviation) at the start of the experiments. Mice were separately housed in a ventilated Scantainer (Scantainer Classic, SCANBUR A/S, Karlslunde, Denmark) under a 12-hour inverted light/dark cycle (lights off at 7:00 a.m. and on at 7:00 p.m.) at a controlled temperature (22-25 °C) and humidity (40-60 %). During behavioral training, mice were held on a food restriction schedule, and their body weight was maintained at 95-85% of their initial body weight. Under the food restriction schedule, mice were given dry food pellets (10-20 % of their body weight) daily at the end of behavioral training. Water was available ad libitum.

Behavioral apparatus

Behavioral testing and recording were conducted on an elevated, dark-toned linear platform measuring 82 cm in length and 10 cm in width (technical drawings are available on https://github.com/GrohLab/A-tactile-discrimination-task-to-study-neuronal-dynamics-in-freely-moving-mice/tree/main/MaterialList) [24], featuring a lick port (LP) at both ends. To access the LPs, mice were required to traverse through an aperture between two aluminum wings mounted onto a motor to adjust the distance between the wings (= aperture width) in each trial. Each LP consisted of a cannula attached to a syringe filled with condensed milk. A piezo sensor, mounted on top of the cannula, detected vibrations and registered lick events. A speaker was mounted close to the LP to deliver white noise. A lick event resulted in either reward delivery (10 µl of condensed milk) or punishment (120 dB white noise, random duration between 1 and 3 seconds) (Fig. 1B). Moreover, three pairs of infrared (IR) sensors were placed along the track, one in the center of the track and the other two in front of the apertures. Three cameras were positioned above the setup: an overview camera, providing a view of the entire

platform, and two high-speed cameras capturing the aperture and LPs for later analysis of whisker movements and touch events (Fig. 1A, Suppl. Videos 1-3). The behavioral apparatus was controlled using Syntalos (Code available at https://github.com/bothlab/syntalos), which controlled the devices and recorded the timing of events (i.e., aperture state, reward/punishment administration, lick detection, and beam crossings of the mice), cameras, electrophysiology, and miniscope signals.

Behavioral paradigm

Mice were trained to perform a go/no-go whisker-dependent paradigm on a linear track (Fig. 1), in which they had to learn to discriminate between apertures of different widths to get a reward and avoid punishment. Mice had to choose the correct response depending on the presented stimulus. The response can either be a lick response (hit for go trials, false alarm [FA] for no-go trials respectively) or to refrain from licking (crossing of middle beam brake) and move on to the subsequent trial (miss for go trials, correct rejection [CR] for no-go trials respectively). Animals were trained on the setup twice per day, each training session lasting 15 minutes, with a break of at least two hours between the two sessions. At the beginning of the session, the mouse was put on the setup at the middle IR beam (Fig. 1A) to start the session. The mouse then runs to one end of the linear track. A trial started when one of the outer IR beams was crossed (Fig. 1A) during the approach to the aperture. Upon sampling the aperture with its whiskers, the mouse has to decide to either lick at the LP or turn and go to the other side of the linear track. A trial ends either after a lick response or, in case the mouse didn't lick, when the mouse crosses the middle point on its way to the other LP. At the beginning of each trial (crossing one of the outer IR beams), the aperture state on the opposite side end of the track was reset randomly. The apertures also perform mock movements when the same aperture was presented twice in a row to avoid any learning due to auditory cues. Table 2 summarizes the stimulus-outcome rules for the different training stages.

Training procedure

The training procedure consisted of several stages, and mice must reach a predetermined criterion in each stage to move on to the next stage (Table 2).

<u>Food restriction, handling, and LP training:</u> One week prior to behavioral training, mice were subjected to food restriction, handling, and LP training. During LP training, a dummy LP was placed in the mouse's home cage, which mimicked the appearance and functionality of the actual LP used in experimental tasks. Whenever the mouse approached the LP to lick, the experimenter manually dispensed condensed milk, as positive reinforcement to associate licking with receiving a reward.

<u>Habituation stage:</u> Milk rewards were presented upon licking alternatingly at each LP in order to encourage mice to run back and forth between the two LPs. Apertures remain in the wide position. Once the mice reached criterion (Table 2), they progressed to the initial rule stage.

<u>Initial rule stage:</u> Go (45 mm "wide") and no-go (25 mm "narrow") apertures were presented with an equal probability of 50 % in a random sequence. Licking upon the go (wide) aperture triggered a reward, and licking at the no-go aperture triggered a punishment (Table 2). Individual mice completed the initial rule stage at an individual point in time, defined by the expert-level criteria (Table 2). For the experiments that involved a gradual decrease in aperture contrast (Fig. 3A), a new aperture width was introduced once the mouse reached the

expert-level criterion or when the mouse performed ≥ 4 sessions and ≥ 500 trials at a performance level below expert-performance threshold (d' = 1.65). The contrast was reduced to a minimum of 2 mm.

Neutral aperture stage: Reward and punishment contingencies remained as in the discrimination stage, but an additional “neutral” aperture (35 mm) was added. Licking upon the neutral aperture resulted in no outcome and no scoring. The neutral aperture stage lasted for 8 sessions (Table 2).

Reversed rule stage: Reward and punishment contingencies were inverted (i.e., the previously rewarded aperture was punished, and vice versa). The neutral aperture was not presented. Individual mice completed the reversed rule stage at an individual point in time, defined by the same expert-level criteria as in the initial rule stage (Table 2).

Extinction stage: Reward and punishment were randomly presented, irrespective of the aperture state. The extinction stage lasted for 8 sessions (Table 2).

Stage name	**Stimulus**	**Response**	**Scoring (outcome)**	**Criterion**
Habituation	45 mm aperture	Lick	Hit (reward)	≥ 4 sessions and ≥ 50 successful lick trials
		No lick	Miss (no outcome)	
Initial rule	45 mm aperture	Lick	Hit (reward)	≥ 4 sessions and ≥ 200 trials above expert-performance threshold (d' = 1.65)
		No lick	Miss (no outcome)	
	25 mm aperture	Lick	FA (punishment)	
		No lick	CR (no outcome)	
Neutral aperture stage	45 mm aperture	Lick	Hit (reward)	8 sessions in total
		No lick	Miss (no outcome)	
	35 mm aperture	Lick	No score (no outcome)	
		No lick	No score (no outcome)	
	25 mm aperture	Lick	FA (punishment)	
		No lick	CR (no outcome)	
Reversed rule	45 mm aperture	Lick	FA (punishment)	

		No lick	CR (no outcome)	≥ 4 sessions and ≥ 200 trials above expert-performance threshold (d' = 1.65)
	25 mm aperture	Lick	Hit (reward)	
		No lick	Miss (no outcome)	
Extinction	45 mm aperture	Lick	No score (random presentation of reward and punishment)	8 sessions in total
		No lick		
	25 mm aperture	Lick		
		No lick		

Table 2: Behavioral paradigm: training stages, stimuli, responses, scoring, outcomes and progression criteria. FA: false alarm; CR: correct rejection.

Data acquisition

Data acquisition during behavior was done with Syntalos [22]. An intan-module recorded all analog signals from the LPs. The overview camera was connected to a recorder module that operated continuously throughout the session. The high-speed cameras and an event list were controlled by a custom-made Python script. The cameras were programmed to start recording when the animal approached the corresponding LP, determined by the crossing of the corresponding light beam. The event list kept track of the triggered light beams and reported the state of the apertures. The list also noted if a trial was a success or failure.

Sensory deprivation protocols (whisker plucking and lidocaine numbing of the whisker pad)

For whisker plucking, mice were anesthetized with 2.5 % isoflurane and then placed in a stereotaxic alignment system (Kopf Instruments) with a mask providing continuous inhalation of 1-2 % isoflurane in medical oxygen. The body temperature was monitored and maintained at 37-39 °C. The mouse's head was tilted to see the whisker pad clearly under the microscope, and lidocaine cream was applied to the whisker pad. The whiskers were then plucked one by one using small cosmetic tweezers. After plucking all the whiskers (on both sides), mice were kept on a heating plate in their preheated cage for a minimum of 30 minutes to recover, and they were given at least 5 hours of rest before their next training session. In a separate sensory deprivation protocol, lidocaine cream was applied topically to the whisker pads during a brief anesthesia with isoflurane approximately 20-30 minutes in advance of the session. For control, neutral ointment (Bepanthen cream) was administered identically. The whiskers remained intact for this intervention.

Electrophysiological recordings

Recording array

Electronic Interface Boards (EIBs) were based on the design developed in [46]. Tetrodes were manufactured in house by folding and twisting approximately 30 cm of tungsten wires (12.5 µm, Item # 100211, Tungsten 99.95% CS Wire, California Fine Wire Company). A total of 16

tetrodes (yielding 64 channels in total) were inserted to a custom-made EIB (produced by Multi-Circuit-Boards). The layout allowed for proper alignment of the tetrodes in the x-y plane. Each tetrode's placement was determined using a scaffold, ensuring precise targeting of BC (5 tetrodes), the VPM (4 tetrodes), the POm (4 tetrodes), and the ZIv (3 tetrodes). Coordinates were defined with respect to bregma, according to [47] (Table 3). After insertion of the tetrodes into the EIB, tetrodes were fixed using UV-curable adhesive (3M™ Filtek™ Supreme XTE, 3M Deutschland GmbH, Neuss, Germany) and the tungsten wires were then soldered onto the copper traces of the EIB. The tetrodes were then suspended in a gold chloride solution (200 mg/dL gold chloride in deionized water, HT1004-100ML, Sigma-Aldrich, Inc., MO, USA) and gold plated to reduce their impedances to less than 100kOhm. To ensure proper conductance of the individual channels, a function generator (A365 Stimulus Isolator, World Precision Instruments, Inc., FL, USA) was connected to a basin filled with sodium chloride (120 mM), in which the tetrodes were submerged. Only EIBs with ≥62 conducting channels were used for implantation.

EIB implantation

30 minutes before inducing general anesthesia, buprenorphine hydrochloride (Bupresol vet. Multidose 0,3 mg/ml, 10 ml, CP-Pharma Handelsgesellschaft mbH, Burgdorf, Germany) was administered subcutaneously at a dosage of 0.1 mg/kg of body weight. General anesthesia was induced using isoflurane (1-2 % in oxygen, Isofluran Baxter, Baxter Deutschland GmbH, Germany), with control of the eyelid reflex and pedal withdrawal reflex. Body temperature was monitored and maintained between 36-38 °C. Eye ointment (Bepanthen®, Bayer, Germany) was applied to the eyes and saline solution (30 ml/kg of body weight, Fresenius Kabi Deutschland GmbH, Bad Homburg, Germany) was administered subcutaneously. Lidocaine (Xylocaine® 1%, Aspen Pharma Trading Limited, Ireland) was injected under the scalp to provide local anesthesia in the surgical area. The animal was positioned in a non-traumatic stereotactic alignment apparatus (David Kopf Instruments, Tujunga, CA, USA). Small holes were drilled in the skull over the target areas using a dental drill (78001 Microdrill, RWD Life Science, TX, USA). The tetrodes were then gradually lowered into the brain until the desired depth was reached. The EIB was secured to the skull using a cyanoacrylate-based adhesive (Super-bond, Sun Medical, Japan) and dental cement (Paladur®, Kulzer, Germany). Following the surgeries, animals were placed into their home cage on a heated surface for a minimum of 2 hours before being returned to the ventilated Scantainer. Behavioral experiments started after an adequate period of recovery following the EIB implantation.

Tetrode	A/P	M/L	D/V with respect to dura
BC 1	**- 1.0**	**3.25**	**- 0.4**
BC 2	**- 1.3**	**3.3**	**- 0.3**
BC 3	**- 1.6**	**2.7**	**- 0.85**
BC 4	**- 1.3**	**2.6**	**- 0.85**
BC 5	**- 1.0**	**2.7**	**- 0.85**
VPM 1	**- 1.95**	**1.95**	**- 2.95**
VPM 2	**- 1.95**	**1.6**	**- 2.95**
VPM 3	**- 1.75**	**1.75**	**- 3.0**
VPM 4	**- 1.45**	**1.6**	**- 2.95**
POm 1	**- 2.15**	**1.3**	**- 2.75**
POm 2	**- 2.3**	**1.5**	**- 2.75**
POm 3	**- 2.3**	**1.15**	**- 2.8**
POm 4	**- 2.0**	**1.05**	**- 2.85**
ZIv 1	**- 2.35**	**2.0**	**- 3.7**
ZIv 2	**- 2.6**	**1.75**	**- 3.7**
ZIv 3	**- 2.15**	**1.75**	**- 3.75**

Table 3: Tetrode Coordinates. BC: barrel cortex; VPM: ventral posteromedial nucleus; POm: posterior medial complex; ZIv: ventral zona incerta.

Histology and identification of tetrode positions

After administering a lethal dose of ketamine-xylazine through intraperitoneal injection (ketamine: 120 mg/kg bw, CP-Pharma Handelsgesellschaft mbH, Burgdorf, Germany; xylazine: 20 mg/kg bw, Xylavet® 20 mg/ml, CP-Pharma Handelsgesellschaft mbH, Burgdorf, Germany), a transcardial perfusion with paraformaldehyde (PFA, 4% in phosphate-buffered saline [PBS]) was performed. The mouse's head, along with the EIB implant, was post-fixed

in PFA (4% in PBS) for five days. Subsequently, the EIB was removed, the brain was cut into 50 µm thick sections with a vibrating microtome (Thermo Scientific Microm HM 650V), and the tetrode traces were identified using a bright field microscope. Tetrode tracks were manually reconstructed from the microscope images using the Amira software (v6.5, Thermo Fisher Scientific, Waltham, MA). Subsequently, all tetrodes located outside of the designated target areas were excluded from further analysis.

Calcium imaging

Viral Injection

For intracranial viral injections, mice were anesthetized with isoflurane (1 - 2%, Univentor 1200 - anesthesia Unit, Univentor, Zejtun, Malta). Mice were head-fixed in a Kopf Stereotax frame (Model 900, David Kopf Instruments, Tujunga, USA). Deep anesthesia was ensured by the absence of the paw pinch reflex. The head was shaved to expose the skin and disinfected with ethanol swabs. The skin was incised along the anterior-posterior axis of the head, and the surface was cleaned with cotton swabs. An oval-shaped craniotomy was made at (M/L: 1.25, A/P: -1.4 to -2.0, D/V: 3.2) mm relative to bregma using a dental drill (EXL-40, Osada Electric co. ltd.). To achieve optimal expression in POm, we injected the virus solution (AAV-1/2-GCaMP6f, 4.4 x 10^{12} GC, 400 nl) at two coordinates (M/L: 1.25, A/P: -1.4, D/V: 3.2; M/L: 1.25, A/P: -2.0, D/V: 3.2). A pulled glass injection pipette (Puller: Model P-97, Sutter Instrument Co., Novato, USA; Pipette: Blaubrand intraMark micropipettes, product ID 708707) loaded with the virus was slowly lowered to the injection site and the virus was slowly injected (~100 nl/min) by manually applying air pressure with an attached syringe. The tissue was allowed to rest for 10 minutes to facilitate diffusion of the virus before the pipette was slowly pulled back up. The skin was sutured back up with a Braun suture kit.

Grin-Lens Implantation

Two to three weeks after the viral injection, the animal was anesthetized and head-fixed on the Stereotax. A small portion of the skin was removed from the head to expose the skull. The connective tissue was removed with cotton swabs. After adjusting the head in the correct 3D plane, a craniotomy was drilled between the previous injections (M/L: 1.25, A/P: -1.7 relative to bregma). A blunt needle was used to make a leading track for the lens. The needle was advanced with a Luigs & Neumann linear actuator by advancing in 300 µm steps and retracting in 200 µm steps at the speed of 30 µm/s to relieve pressure to a final depth of 3000 µm from the dura. The GRIN lens (Inscopix, product code 1050-004627, ProView™ Lens Probe, 0.5 mm diameter, ~4.0 mm length) was held with a 3D printed custom lens holder. The lens was lowered slowly in the same way as the blunt needle, except for the final depth being 3100 µm . The lens was then fixed to the skull with a self-curing resin cement (Super-bond, Sun Medical, Japan).

Baseplate Implantation

After the GRIN lens implantation, a baseplate was attached to a miniscope, which was lowered while acquiring images through the GRIN lens. The baseplate was lowered to the focal plane and then fixed to the skull with UV-cured dental cement (Gradia Direct Flo, A3, GC Corporation).

Data analysis

The behavioral data was analyzed using custom code developed in MATLAB R2023a (The MathWorks, Inc.), which is available on A-tactile-discrimination-task-to-study-neuronal-

dynamics-in-freely-moving-mice/DataAndScripts at main · GrohLab/A-tactile-discrimination-task-to-study-neuronal-dynamics-in-freely-moving-mice · GitHub [24]. P-values ≤ 0.05 were considered significant. Mean values were reported with standard deviations and median values with interquartile range (IQR).

Statistical analysis of the learning process

Task performance in each session was measured using the discriminability index d-prime (d'), also known as Fisher discrimination index [48,49]. The d' is a statistical measure to quantify the ability to discriminate between signal and noise and is defined as the difference between the z-scores of the hit rate and the FA rate: $d' = z(hit\ rate) - z(false\ alarm\ rate)$. Due to the constraints of the z-score transformation (which cannot handle proportions of 0 or 1), hit rates and FA rates of 0 are typically adjusted to $(\frac{1}{2*n})$ and rates of 1 are adjusted to $(1 - \frac{1}{2*n})$, with n being the number of go- (for hit rate adjustment), or no-go trials (for FA rate adjustment), respectively. A higher d' indicates greater discriminability, meaning the observer can more effectively distinguish signal from noise. A d' of 0 describes a discrimination performance at chance level. An animal was considered to reach expert performance when it crossed a d' of 1.65, corresponding to a one-tailed significance level of α = 0.05.

Extraction of behavioral data from videos

Spatial information of the mice was extracted from video recordings using DeepLabCut [23]. Following preprocessing with median background image subtraction, the DeepLabCut model was trained on a subset of manually annotated video frames. For the high-speed videos, these markers consisted of 8 data points for two whiskers on each side from whisker base to tip and markers for the mouse's head contours. In overview videos, spatial positioning and velocity were estimated based on anatomical landmarks on the mouse's body and head. For the positional data analysis (Fig. 4D), the linear track was divided into rectangles measuring 10 mm by 1 mm. The time spent in each area was calculated by counting the number of video frames in which the mouse was present within each specific rectangle.

Electrophysiological data

The raw electrophysiological data was spike-sorted with KiloSort 2.0. Subsequently, the sorted clusters were curated automatically using the Ecephys spike sorting algorithm provided by the Allen Brain Observatory (code available at https://github.com/alleninstitute/ecephys_spike_sorting). The algorithm includes noise templates to identify and exclude clusters exhibiting characteristics indicative of noise, such as irregular waveform shapes and interspike interval (ISI) histograms. The following quality metrics were then applied to further exclude any clusters indicative of multi-unit activity: isolation distance (computed from Mahalanobis distance) greater than 15 and ISI violation below 3 %, with an ISI threshold of 1.5 milliseconds. The criteria were selected based on previous studies [50–52], where they have been demonstrated to effectively distinguish well-isolated single units from noise and multi-unit activity. The individual units were further classified into fast spiking (FS) and regular spiking (RS) units, putatively representing inhibitory and excitatory neurons, respectively (Barthó et al., 2004). The threshold for differentiating RS from FS units was set to a trough-to-peak duration of 350 µs for cortex and zona incerta, and 300 µs for thalamic nuclei. These thresholds align with previous studies (Barthó et al., 2014; Mahrach et al., 2020) and consider the fact that extracellular waveforms in the thalamus are

shorter than those in the cortex (Barthó et al., 2014). For further analysis, only RS units were selected for BC, VPM, and POm, while FS units were selected for ZIv.

Extraction of Calcium Traces and Spatial Footprints

The preprocessing, motion correction, and extraction of the calcium traces and spatial footprints from the videos was done with Minian [53]. All downstream processing was done using custom code developed in MATLAB R2023a (The MathWorks, Inc.).

Touch modulated neurons

Calcium transients of the POm neurons were extracted in a window of 400 ms before and after the whisker touch (see above). The summed calcium activity before and after the touch was compared with a paired two-tailed t-test. Whisker touch responsiveness for the extracellular recordings was determined by a statistically significant increase in firing rates (to either of the two aperture states) within a 200 ms response window following aperture touch, compared to a baseline window preceding touch onset. Statistical significance was determined by a two-sample Kolmogorov-Smirnov test. Those units which showed significant differences were identified as touch-modulated neurons.

Decoding of aperture width form unit spike trains

Aperture width decoding from unit spike trains traces was conducted using the Neural Decoding Toolbox [54]. The dataset was partitioned into a training set (90% of labels) and a test set (10% of labels). Each set contained the spike traces of individual units for a given trial and the corresponding aperture labels. A support vector machine (SVM) classifier was trained using the LIBSVM software package. The classifier was subjected to a 10-fold cross-validation, where it was trained and tested on different data partitions. The mean decoding accuracy was then calculated over a window from trigger onset to 400 ms post-trigger onset.

Decoding of aperture width from whisker angles

Aperture width decoding from whisker angles was performed using MATLAB's built-in generalized additive model (GAM) classifier. The dataset was partitioned into a training set (80% of labels) and a test set (20% of labels). Each set included whisker angles recorded 20 frames before and 100 frames after whisker touch, with a sampling rate of 240 fps, along with the corresponding aperture labels. In the shuffled decoding accuracy analysis, the whisker angle traces were randomly allocated to an aperture label. P-values were determined using pointwise 95% confidence intervals, which were computed by the MATLAB "rocmetrics" function based on 100 pointwise bootstrap resamples.

Data availability

https://github.com/GrohLab/A-tactile-discrimination-task-to-study-neuronal-dynamics-in-freely-moving-mice/tree/main/DataAndScripts/RawData [24]

Code availability

https://github.com/GrohLab/A-tactile-discrimination-task-to-study-neuronal-dynamics-in-freely-moving-mice/tree/main/DataAndScripts [24]

References

1. Temereanca, S. & Simons, D. J. Functional topography of corticothalamic feedback enhances thalamic spatial response tuning in the somatosensory whisker/barrel system. *Neuron* **41**, 639–651 (2004).
2. Larkum, M. E., Zhu, J. J. & Sakmann, B. A new cellular mechanism for coupling inputs arriving at different cortical layers. *Nature* **398**, 338–341 (1999).
3. Bruno, R. M. & Sakmann, B. Cortex is driven by weak but synchronously active thalamocortical synapses. *Science* **312**, 1622–1627 (2006).
4. Mease, R. A., Krieger, P. & Groh, A. Cortical control of adaptation and sensory relay mode in the thalamus. *Proc. Natl. Acad. Sci. U. S. A.* **111**, 6798–6803 (2014).
5. Poulet, J. F. A. & Petersen, C. C. H. Internal brain state regulates membrane potential synchrony in barrel cortex of behaving mice. *Nature* **454**, 881–885 (2008).
6. Banerjee, A. *et al.* Value-guided remapping of sensory cortex by lateral orbitofrontal cortex. *Nature* **585**, 245–250 (2020).
7. Huber, D. *et al.* Sparse optical microstimulation in barrel cortex drives learned behaviour in freely moving mice. *Nature* **451**, 61–64 (2008).
8. de Kock, C. P. J. & Sakmann, B. Spiking in primary somatosensory cortex during natural whisking in awake head-restrained rats is cell-type specific. *Proc. Natl. Acad. Sci. U. S. A.* **106**, 16446–16450 (2009).
9. Oberlaender, M., Ramirez, A. & Bruno, R. M. Sensory experience restructures thalamocortical axons during adulthood. *Neuron* **74**, 648–655 (2012).
10. Moore, J. D. *et al.* Hierarchy of orofacial rhythms revealed through whisking and breathing. *Nature* **497**, 205–210 (2013).
11. Borden, P. Y. *et al.* Thalamic bursting and the role of timing and synchrony in thalamocortical signaling in the awake mouse. *Neuron* **110**, 2836–2853.e8 (2022).
12. Ahissar, E., Sosnik, R. & Haidarliu, S. Transformation from temporal to rate coding in a somatosensory thalamocortical pathway. *Nature* **406**, 302–306 (2000).
13. Woolsey, T. A. & Van der Loos, H. The structural organization of layer IV in the somatosensory region (SI) of mouse cerebral cortex. The description of a cortical field composed of discrete cytoarchitectonic units. *Brain Res.* **17**, 205–242 (1970).
14. Xu, N.-L. *et al.* Nonlinear dendritic integration of sensory and motor input during an active sensing task. *Nature* **492**, 247–251 (2012).
15. Petreanu, L. *et al.* Activity in motor-sensory projections reveals distributed coding in somatosensation. *Nature* **489**, 299–303 (2012).
16. Sachidhanandam, S., Sreenivasan, V., Kyriakatos, A., Kremer, Y. & Petersen, C. C. H. Membrane potential correlates of sensory perception in mouse barrel cortex. *Nat. Neurosci.* **16**, 1671–1677 (2013).
17. Chen, J. L., Carta, S., Soldado-Magraner, J., Schneider, B. L. & Helmchen, F. Behaviour-dependent recruitment of long-range projection neurons in somatosensory cortex. *Nature* **499**, 336–340 (2013).
18. Rodgers, C. C. *et al.* Sensorimotor strategies and neuronal representations for shape discrimination. *Neuron* **109**, 2308–2325.e10 (2021).
19. Hong, Y. K., Lacefield, C. O., Rodgers, C. C. & Bruno, R. M. Sensation, movement and learning in the absence of barrel cortex. *Nature* **561**, 542–546 (2018).
20. Krupa, D. J., Matell, M. S., Brisben, A. J., Oliveira, L. M. & Nicolelis, M. A. L. Behavioral Properties of the Trigeminal Somatosensory System in Rats Performing Whisker-Dependent Tactile Discriminations. *J. Neurosci.* **21**, 5752–5763 (2001).
21. Krupa, D. J., Wiest, M. C., Shuler, M. G., Laubach, M. & Nicolelis, M. A. L. Layer-specific somatosensory cortical activation during active tactile discrimination. *Science* **304**, 1989–1992 (2004).
22. Klumpp, M. *et al.* Syntalos: A software for precise simultaneous multi-modal data acquisition and closed-loop interventions. *Research Square* (2024) doi:10.21203/rs.3.rs-3793251/v1.
23. Mathis, A. *et al.* DeepLabCut: markerless pose estimation of user-defined body parts

with deep learning. *Nat. Neurosci.* **21**, 1281–1289 (2018).
24. Heimburg, F., Saluti, N. M., Timm, J., Adlakha, A., Castelanelli, M., Klumpp M., Embray L., Both M., Draguhn A., Kuner T., Groh A. *Supplementary Materials for 'A Tactile Discrimination Task to Study Neuronal Dynamics in Freely-Moving Mice' (2024)*. doi:10.5281/zenodo.13369686.
25. Suzuki, M. & Larkum, M. E. General anesthesia decouples cortical pyramidal neurons. *Cell* **180**, 666–676.e13 (2020).
26. Sumser, A., Isaias-Camacho, E., Mease, R. A. & Groh, A. Differential representation of active and passive touch in mouse somatosensory thalamus. *bioRxiv* 2024.07.16.603697 (2024) doi:10.1101/2024.07.16.603697.
27. La Terra, D. *et al.* The role of higher-order thalamus during learning and correct performance in goal-directed behavior. *Elife* **11**, (2022).
28. Qi, J., Ye, C., Naskar, S., Inácio, A. R. & Lee, S. Posteromedial thalamic nucleus activity significantly contributes to perceptual discrimination. *PLoS Biol.* **20**, e3001896 (2022).
29. Mo, C., McKinnon, C. & Murray Sherman, S. A transthalamic pathway crucial for perception. *Nat. Commun.* **15**, 1–13 (2024).
30. Mitchinson, B. *et al.* Active vibrissal sensing in rodents and marsupials. *Philos. Trans. R. Soc. Lond. B Biol. Sci.* **366**, 3037–3048 (2011).
31. Lou, Y., Caruana, R. & Gehrke, J. Intelligible models for classification and regression. in *Proceedings of the 18th ACM SIGKDD international conference on Knowledge discovery and data mining* 150–158 (Association for Computing Machinery, New York, NY, USA, 2012). doi:10.1145/2339530.2339556.
32. Gilad, A., Gallero-Salas, Y., Groos, D. & Helmchen, F. Behavioral Strategy Determines Frontal or Posterior Location of Short-Term Memory in Neocortex. *Neuron* **99**, 814–828.e7 (2018).
33. Isett, B. R., Feasel, S. H., Lane, M. A. & Feldman, D. E. Slip-Based Coding of Local Shape and Texture in Mouse S1. *Neuron* **97**, 418–433.e5 (2018).
34. Park, J. M. *et al.* Deep and superficial layers of the primary somatosensory cortex are critical for whisker-based texture discrimination in mice. *bioRxiv* 2020.08.12.245381 (2020) doi:10.1101/2020.08.12.245381.
35. Oladazimi, M., Brendel, W. & Schwarz, C. Biomechanical Texture Coding in Rat Whiskers. *Sci. Rep.* **8**, 11139 (2018).
36. Ghane-Motlagh, B. & Sawan, M. Design and implementation challenges of microelectrode arrays: A review. *Mater. Sci. Appl.* **04**, 483–495 (2013).
37. Ward, M. P., Rajdev, P., Ellison, C. & Irazoqui, P. P. Toward a comparison of microelectrodes for acute and chronic recordings. *Brain Res.* **1282**, 183–200 (2009).
38. Geng, J. *et al.* Chronic Ca2+ imaging of cortical neurons with long-term expression of GCaMP-X. *Elife* **11**, (2022).
39. Darainy, M., Manning, T. F. & Ostry, D. J. Disruption of somatosensory cortex impairs motor learning and retention. *J. Neurophysiol.* **130**, 1521–1528 (2023).
40. Morehead, J. R., Qasim, S. E., Crossley, M. J. & Ivry, R. Savings upon re-aiming in visuomotor adaptation. *J. Neurosci.* **35**, 14386–14396 (2015).
41. Hooks, B. M. *et al.* Organization of cortical and thalamic input to pyramidal neurons in mouse motor cortex. *J. Neurosci.* **33**, 748–760 (2013).
42. Jadhav, S. P., Wolfe, J. & Feldman, D. E. Sparse temporal coding of elementary tactile features during active whisker sensation. *Nat. Neurosci.* **12**, 792–800 (2009).
43. Wolfe, J. *et al.* Texture coding in the rat whisker system: slip-stick versus differential resonance. *PLoS Biol.* **6**, e215 (2008).
44. Zuo, Y., Perkon, I. & Diamond, M. E. Whisking and whisker kinematics during a texture classification task. *Philos. Trans. R. Soc. Lond. B Biol. Sci.* **366**, 3058–3069 (2011).
45. Schwarz, C. *et al.* The head-fixed behaving rat--procedures and pitfalls. *Somatosens. Mot. Res.* **27**, 131–148 (2010).
46. Oettl, L.-L. *et al.* Phasic dopamine reinforces distinct striatal stimulus encoding in the olfactory tubercle driving dopaminergic reward prediction. *Nat. Commun.* **11**, 3460 (2020).

47. Paxinos, G. & Franklin, K. B. J. The mouse brain in stereotaxic coordinates. San Diego, Calif. Preprint at (2001).
48. Stanislaw, H. & Todorov, N. Calculation of signal detection theory measures. *Behav. Res. Methods Instrum. Comput.* **31**, 137–149 (1999).
49. Macmillan, N. A. & Douglas Creelman, C. *Detection Theory: A User's Guide*. (CUP Archive, 1991).
50. Onodera, K. & Kato, H. K. Translaminar recurrence from layer 5 suppresses superficial cortical layers. *Nat. Commun.* **13**, 2585 (2022).
51. Rosenberg, D. M. & Horn, C. C. Neurophysiological analytics for all! Free open-source software tools for documenting, analyzing, visualizing, and sharing using electronic notebooks. *J. Neurophysiol.* **116**, 252–262 (2016).
52. Trautmann, E. M. *et al.* Accurate Estimation of Neural Population Dynamics without Spike Sorting. *Neuron* **103**, 292–308.e4 (2019).
53. Dong, Z. *et al.* Minian, an open-source miniscope analysis pipeline. *Elife* **11**, (2022).
54. Meyers, E. M. The neural decoding toolbox. *Front. Neuroinform.* **7**, 8 (2013).

Acknowledgments

We thank Katharina Ziegler for helpful comments on the manuscript. We thank Wolfgang Kelsch and Max Scheller for teaching us the electronic interface board approach as well as Cornelius Schwarz for providing us with the lick ports. This work was supported by the German Research Foundation (DFG Grants GR3757/4-1 to AG and KU 1983/8-1 to TK). We acknowledge the data storage service SDS@hd and high-performance computing initiative bwHPC, supported by the Ministry of Science, Research and the Arts Baden-Württemberg (SDS@hd and bwHPC) and the German Research Foundation (DFG) through grant INST 35/1314-1 FUGG and INST 35/1503-1 FUGG (SDS@hd). The funders had no role in study design, data collection and analysis, decision to publish, or preparation of the manuscript.

Author information

Authors and Affiliations

Institute for Physiology and Pathophysiology, Heidelberg University, 69120, Germany

Filippo Heimburg, Josephine Timm, Nadin Mari Saluti, Melina Castelanelli, Matthias Klumpp, Lee Embray, Martin Both, Andreas Draguhn and Alexander Groh

Institute for Anatomy and Cell Biology, Heidelberg University, 69120, Germany

Avi Adlakha and Thomas Kuner

Institute for Experimental Epileptology and Cognition Research, University of Bonn, 53105, Germany

Current affiliation: Josephine Timm

Contributions

F.H., J.T., N.S., M.C. and A.G. designed the experiments. L.E., F.H., N.S., M.K. and M.C. constructed the setup under supervision of A.G.. M.K. developed Syntalos under supervision of M.B. and A.D.. J.T., F.H., N.S. and A.A. collected the data and analyzed the data under supervision of A.G.. J.T., F.H., N.S., A.A. and A.G. wrote the paper.

Corresponding author
Correspondence to Alexander Groh

Ethics declarations

Competing interests
The authors declare no competing interests.

Extended data figures and tables

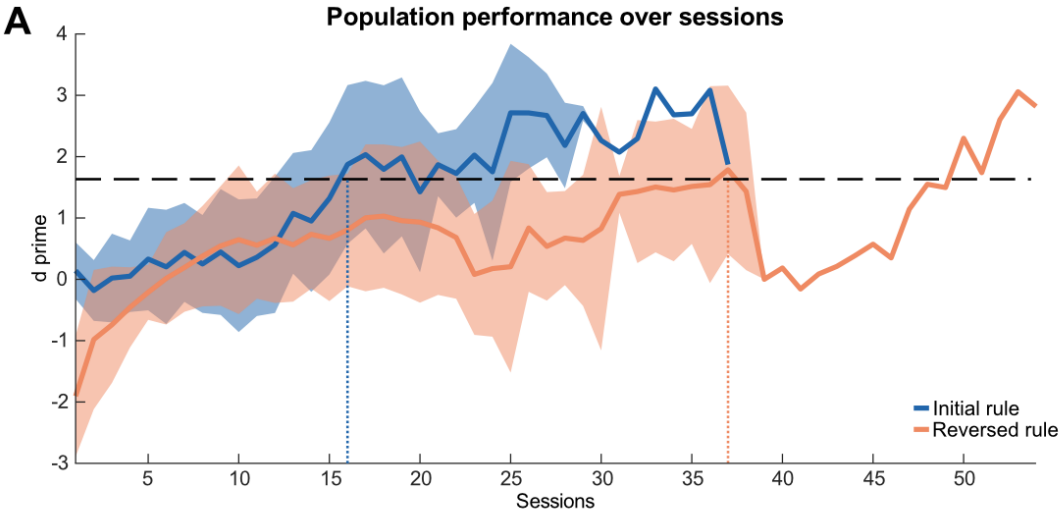

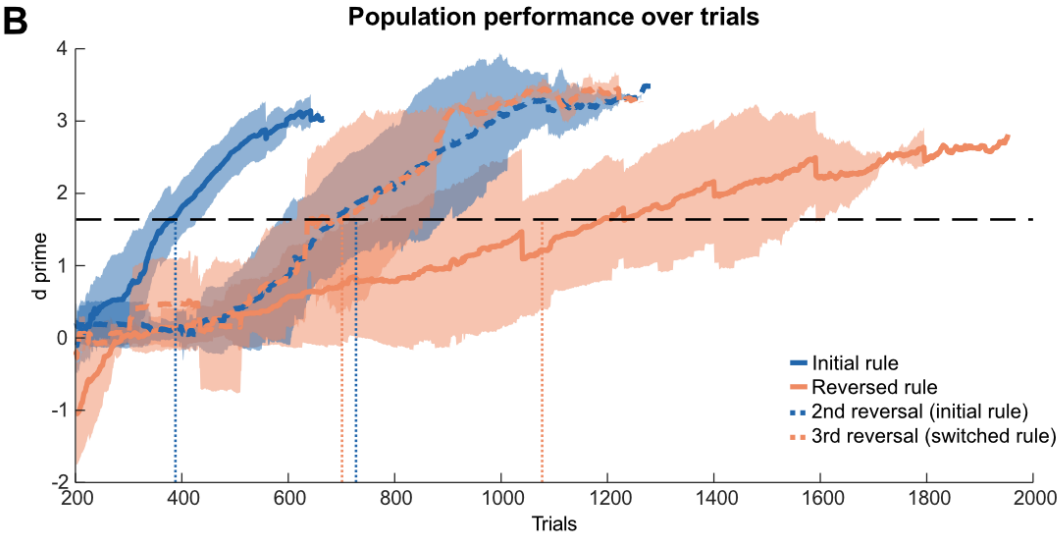

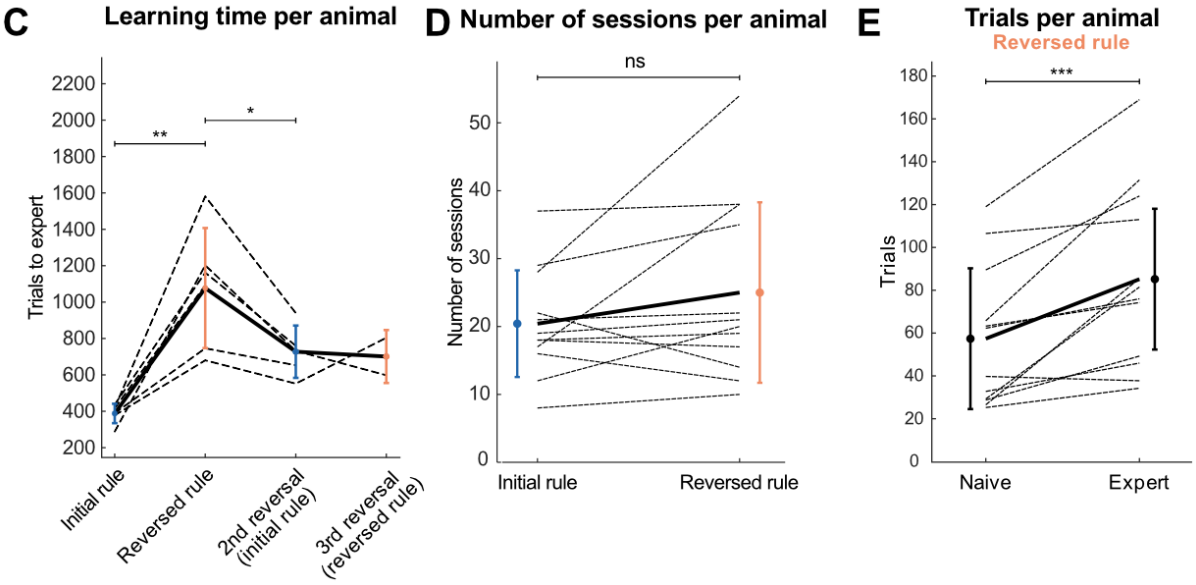

Supplementary Fig. 1: Learning curves for initial and repeated rule reversals. **A:** Population performance over sessions for a contrast of 20 mm. Solid lines show mean d'; shaded areas show standard deviation (initial rule: blue and reversed rule: orange; horizontal line: expert-level performance threshold (d' = 1.65); n = 12 mice). Animals reached expert-level performance after 16 sessions in the initial rule stage and after 37 sessions in the reversed rule stage (dotted vertical lines). **B:** Population performance over trials for initial-, 1st- 2nd- and 3rd- rule reversal. Mean d' calculated with a running window of the preceding 200 trials; shaded areas show standard deviation (initial rule: blue and reversed rule: orange; dashed lines: repeated rule switches; horizontal line: expert-level performance threshold (d' = 1.65); n = 6 mice). Animals reached expert-level performance after 388 trials in the initial rule stage, after 1077 trials in the reversed rule stage, after 728 trials in the 2nd reversal and after 701 trials in the 3rd reversal (dotted vertical lines). **C:** Learning times for initial-, 1st-, 2nd- and 3rd- rule reversal (dotted lines: individual animals; solid lines: means and standard deviation; n = 6 mice). **D:** Number of sessions per animal for the initial and reversed rule. (dotted lines: individual animals; solid lines: means and standard deviation; n = 12 mice). **E:** Trials per session during the reversed rule stage for naive and expert animals (dotted lines: individual animals; solid lines: means and standard deviation; n = 12 mice).

ns: $p > 0.05$, *: $p \leq 0.05$, **: $p \leq 0.01$ and ***: $p \leq 0.001$; C-E: paired t-test.

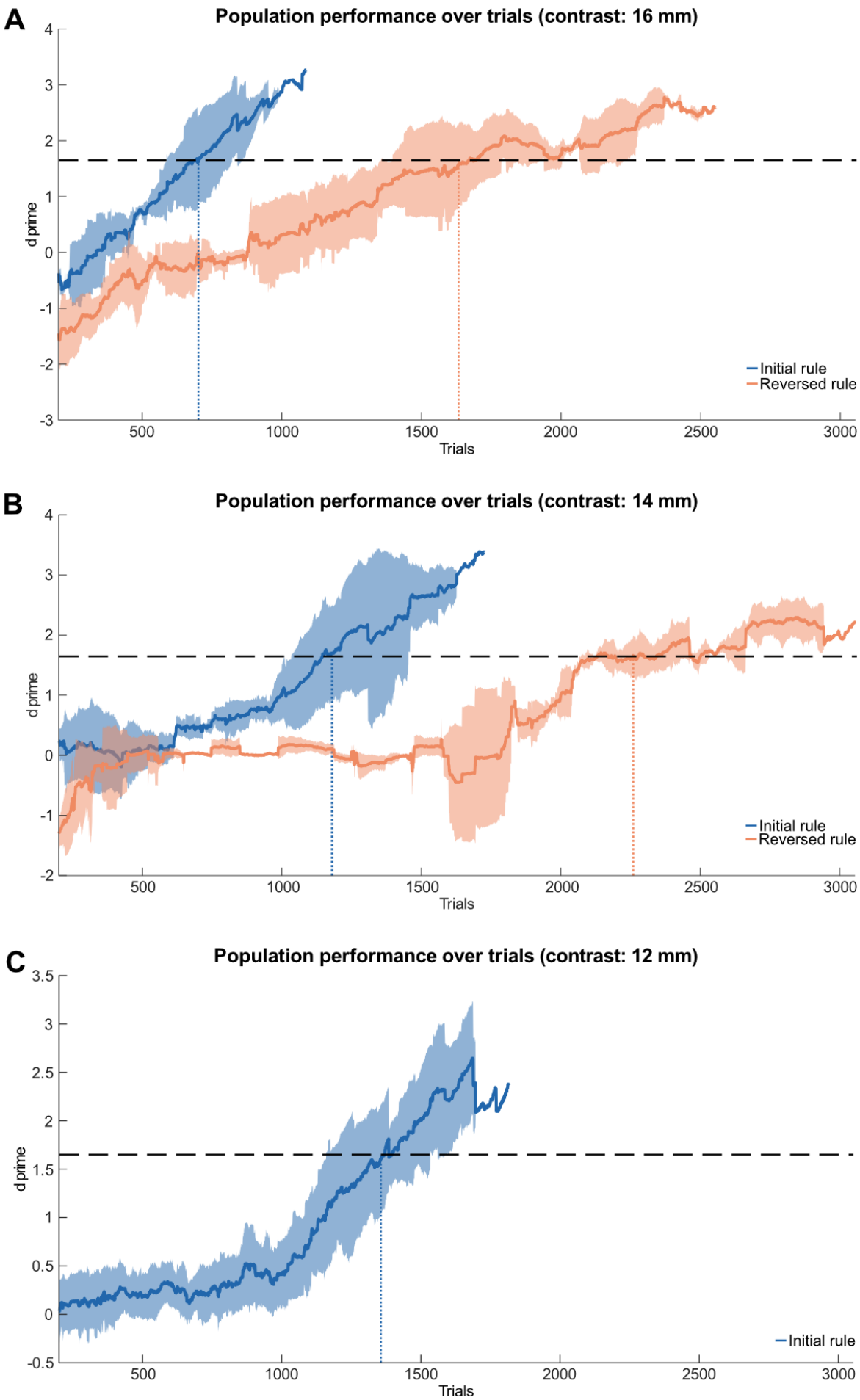
A
Population performance over trials (contrast: 16 mm)
d prime
Trials
Initial rule
Reversed rule
B
Population performance over trials (contrast: 14 mm)
d prime
Trials
Initial rule
Reversed rule
C
Population performance over trials (contrast: 12 mm)
d prime
Trials
Initial rule

Supplementary Fig. 2: Learning curves for different contrasts. **A:** Population performance over trials for 16 mm contrast. Solid lines show mean d', calculated with a running window of the preceding 200 trials; shaded areas show standard deviation (initial rule: blue and reversed rule: orange; horizontal line: expert-level performance threshold (d' = 1.65); n = 3 mice). Animals reached expert-level performance after 701 trials in the initial rule stage and after 1633 trials in the reversed rule stage (dotted vertical lines). **B:** Same as in A for 14 mm contrast (n = 3 mice (initial rule) and 2 mice (reversed rule)). Animals reached expert-level performance after 1180 trials in the initial rule stage and after 2260 trials in the reversed rule stage (dotted vertical lines). **C:** Same as in A, B for 12 mm contrast (n = 6 mice). Animals reached expert-level performance after 1356 trials in the initial rule stage (dotted vertical line).

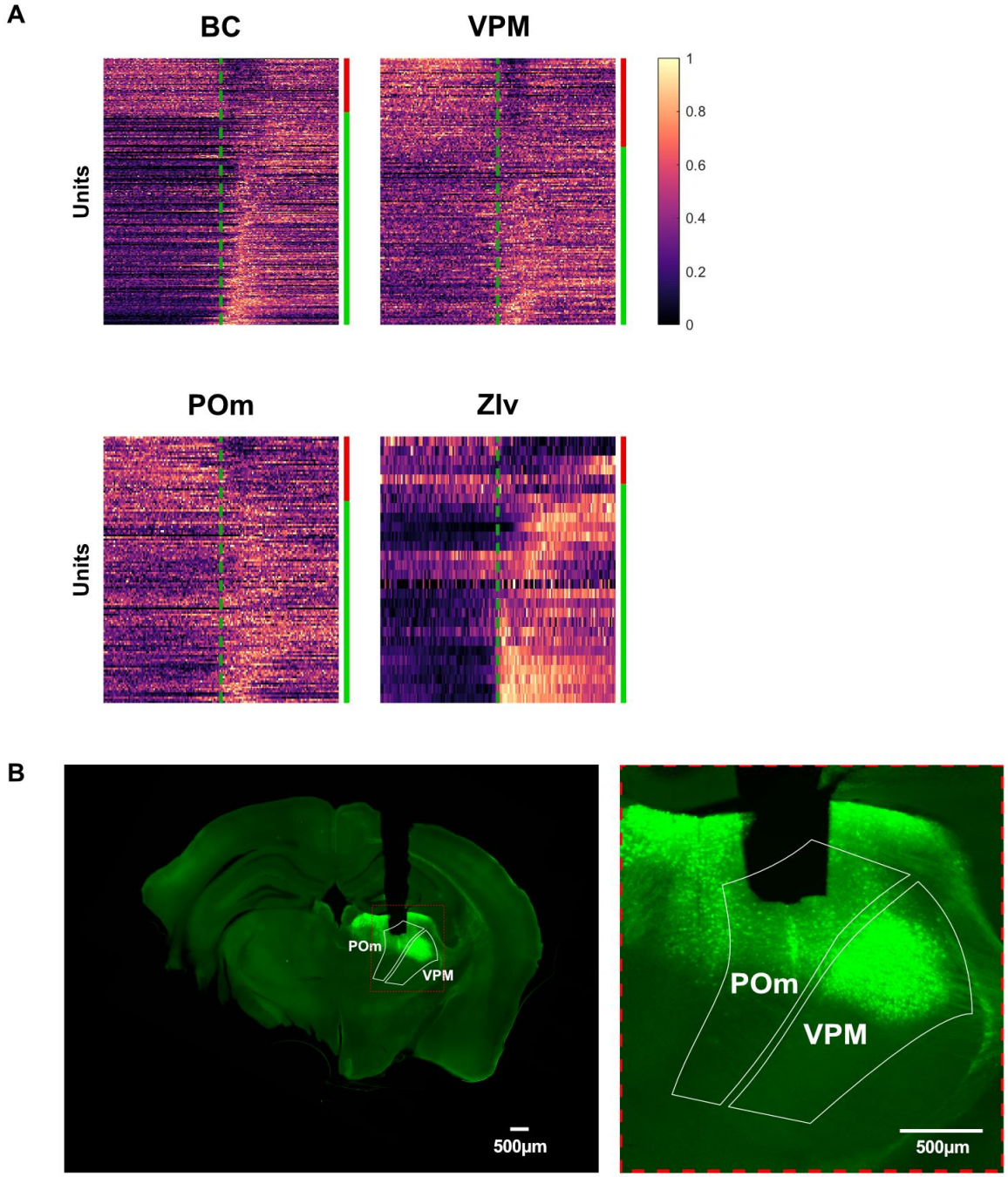

Supplementary Fig. 3: Multisite tetrode recordings and miniscope imaging during aperture discrimination learning task. **A:** Colored PSTHs of all touch-modulated units for each recorded brain area (BC, VPM, POm, and ZIv) aligned to the whisker touch of the aperture (green). Firing frequencies were min-max normalized to a range of 0 to 1 for each unit. Units were ranked in ascending order from top to bottom based on their response magnitude within the response window (200 ms following aperture touch). The bars to the side indicate the proportion of depressed (red) and excited (green) units. The number of units analyzed per region were as follows: BC (n = 261; 53 depressed, 208 excited), VPM (n = 189; 63 depressed, 126 excited), POm (n = 128; 31 depressed, 97 excited), and ZIv (n = 28; 5 depressed, 23 excited). **B:** Left: Coronal section of example mouse brain slice, indicating the tract of the GRIN lens, and the recording region for GCamp6f (green) calcium imaging in POm. Right: same as left at higher magnification.

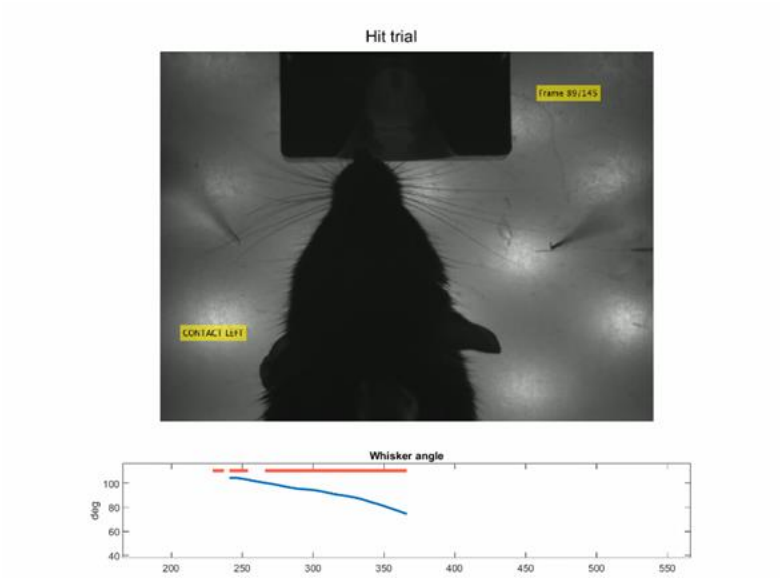

Supplementary video 1: High-speed camera video depicting a hit trial, recorded at 240 FPS and slowed down by a factor of 10 for video playback. The mouse identifies the rewarded aperture and licks lick port to obtain the reward. The accompanying plots display: (1) the average whisker angle relative to the whisker pad (protraction indicated by greater whisker angles), (2) the head angle relative to the midline (values >0° indicate a rightward tilt), and (3) the velocity of the mouse's head within the field of view.

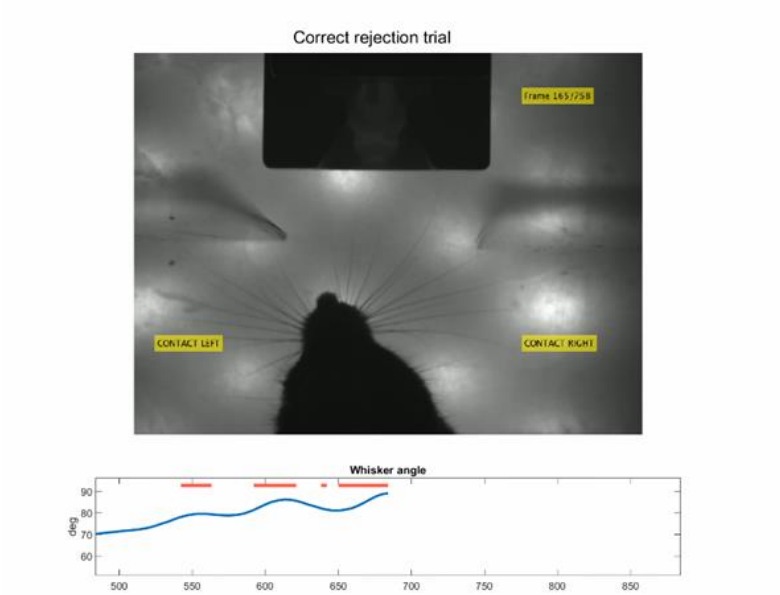

Supplementary video 2: High-speed camera video depicting a correct rejection (CR) trial, recorded at 240 FPS and slowed down by a factor of 10 for video playback. The mouse identifies the punished aperture and turns away from the lick port. The accompanying plots display: (1) the average whisker angle relative to the whisker pad (protraction indicated by greater whisker angles), (2) the head angle relative to the midline (values >0° indicate a rightward tilt), and (3) the velocity of the mouse's head within the field of view.

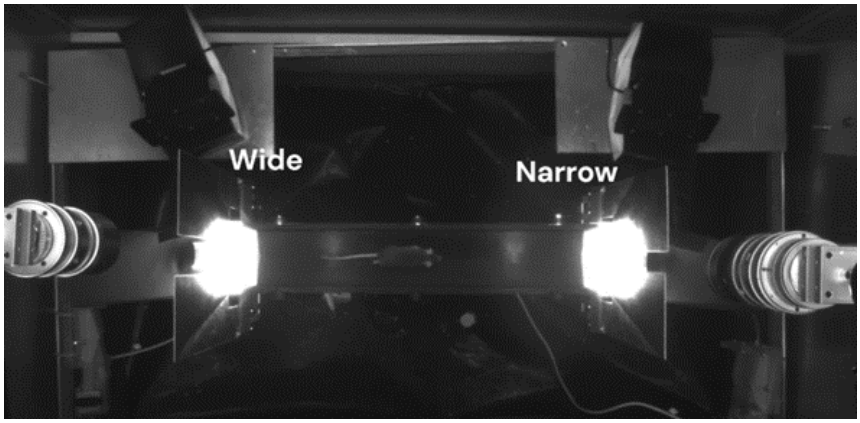

Supplementary video 3: Overview camera video illustrating the experimental setup, recorded at 60 FPS and accelerated by a factor of 2 during video playback. The mouse alternately navigates a linear track to obtain rewards and avoid punishments based on the aperture state. The aperture state, determined by the width of the wing's cleft, changes automatically and randomly between two states. Speakers for administering punishment were positioned behind the linear track. High-speed cameras were positioned overhead at the reward retrieval sites to track whisker-aperture interactions during stimulus sampling.

Figure	Groups	Test statistic, p values, 95% confidence interval (95%CI)	Statistical test
2B	Naive vs. expert sessions (initial rule)	t-statistic = -5.4562, p = 1.99×10^{-4}, 95%CI of the true mean difference = [-61.369; -26.0893]	two-tailed, paired t-test
2C	Initial vs. reversed rule intercept	t-statistic = -7.1879, p = $1{,}78 \times 10^{-5}$, 95%CI of the true mean difference = [-825.9572; -438.7095]	two-tailed, paired t-test
2D	Initial vs. reversed rule slope	t-statistic = 3.4331, p = 0.0056, 95%CI of the true mean difference = [0.0012; 0.0053]	two-tailed, paired t-test
2E	Initial vs. extinction sessions	F-statistic = 2171.411, p = 0.000, 95%CI of the true mean difference = [2.241; 2.923]	repeated measures anova
2E	Reversed vs. extinction sessions	F-statistic = 2171.411, p = 0.000, 95%CI of the true mean difference = [1.869; 2.732]	repeated measures anova
2F	Backlights on vs. backlights off	F-statistic = 0.009, p = 0.926, 95%CI of the true mean difference = [-0.728; 0.488]	repeated measures anova
2G	Bepanthen vs. lidocaine sessions	t-statistic = 3.9892, p = 0.0282, 95%CI of the true mean difference = [0.3585; 3.1870]	two-tailed paired t-test with means for each animal
2H	Pre pluck vs. post pluck	t-statistic = 13.6362, p = 3.8×10^{-5}, 95%CI of the true mean difference = [1.9665; 2.8802]	two-tailed, paired t-test

3B	Initial vs. reversed rule intercept (contrats = 20)	t-statistic = -7.1879, p = $1{,}77 \times 10^{-5}$, 95%CI of the true mean difference = [-825.9572; -438.7095]	two-tailed, paired t-test
3B	Initial vs.reversed rule intercept (contrats = 16)	t-statistic = -5.7857, p = 0.0286, 95%CI of the true mean difference = [-1625.68; -238.9859]	two-tailed, paired t-test
4C	Lick latencies in the different trial quarters of the initial learning stage	Chi-sq = 327.82, p = 9.4617×10^{-71} quarter 1 vs. quarter 2, p = 1.3660×10^{-8} quarter 1 vs. quarter 3, p = 0.0000 quarter 1 vs. quarter 4, p = 0.0000	Friedman test Dunn-Sidak-Adjusted Multiple Comparisons
6B	Naive CR vs. naive FA	p = 2.3356×10^{-8}	two-tailed Wilcoxon rank sum test
6B	Expert CR vs. expert FA	p = 0.5762	two-tailed Wilcoxon rank sum test
6B	Naive CR vs. expert CR	p = 1.7981×10^{-6}	two-tailed Wilcoxon rank sum test
6B	Naive FA vs. expert FA	p = 0.2900	two-tailed Wilcoxon rank sum test
6D	Lidocaine sessions Control sessions Shuffled labels	Mean AUC = 0.8687, 95%CI = [0.8207, 0.9050] Mean AUC = 0.9059, 95%CI = [0.8590, 0.9304] Mean AUC = 0.5303, 95%CI = [0.4580, 0.6216]	
6D	Lidocaine vs. control	t-statistic = -1.6676, p = 0.0972	two-tailed, two-sample t-test
6D	Control vs. shuffled	t-statistic = 7.7886, p = 3.5392×10^{-12}	two-tailed, two-sample t-test
6D	Lidocaine vs. shuffled	t-statistic = 6.7526, p = 4.4247×10^{-10}	two-tailed, two-sample t-test
6E	BC	t-statistic = 9.2115, p = 9.2337×10^{-5}, 95%CI of the true mean difference = [15.9986; 27.5728]	two-tailed, paired t-test
6E	VPM	t-statistic = 8.4932, p = 1.4578×10^{-4}, 95%CI of the true mean difference = [10.2717; 18.5855]	two-tailed, paired t-test
6E	POm	t-statistic = 3.2869, p = 0.0167, 95%CI of the true mean difference = [2.7197; 18.5660]	two-tailed, paired t-test
6E	ZIv	t-statistic = 4.1617, p = 0.0059, 95%CI of the true mean difference = [4.4735; 17.2408]	two-tailed, paired t-test

S1C	Initial vs. reversed rule intercept (repeated rule switch cohort)	t-statistic = -5.1440, p = 0.0036, 95%CI of the true mean difference = [-1033.31; -344.6872]	two-tailed, paired t-test
S1C	Reversed vs. 2nd reversal rule intercept (repeated rule switch cohort)	t-statistic = 3.3183, p = 0.0294, 95%CI of the true mean difference = [56.5671; 636.2329]	two-tailed, paired t-test
S1D	Initial vs reversed number of sessions	t-statistic = -1.6198, p = 0.1336, 95%CI of the true mean difference = [-10.8114; 1.6447]	two-tailed paired t-test
S1E	Naive vs. expert sessions (switched rule)	t-statistic = -4.126, p = 0.0017, 95%CI of the true mean difference = [-42.6171; -12.9663]	two-tailed paired t-test

Supplementary table 1. Description of statistical parameters.